Medical Physics
Introduction to Medical Imaging

ASP 2022
**Peyton Irmen, MMP, DABR; Inova Health System**
Kelly Kisling, PhD, DABR; University of California San Diego Health

- **Computed Tomography (CT)**

- **Positron Emission Tomography (PET)**

- **Magnetic Resonance Imaging (MRI)**

Computed Tomography

- Projection Radiography
  - 3-dimensional structure of an object (anatomy of a patient) can be reduced to a 2-dimensional representation
 - The representation is a display of the linear attenuation through a patient

kV $Radiograph, Ankle$

Source

$\mu_1 t_1$ $\mu_2 t_2$ $\mu_3 t_3$ $\mu_4 t_4$ $\mu_n t_n$
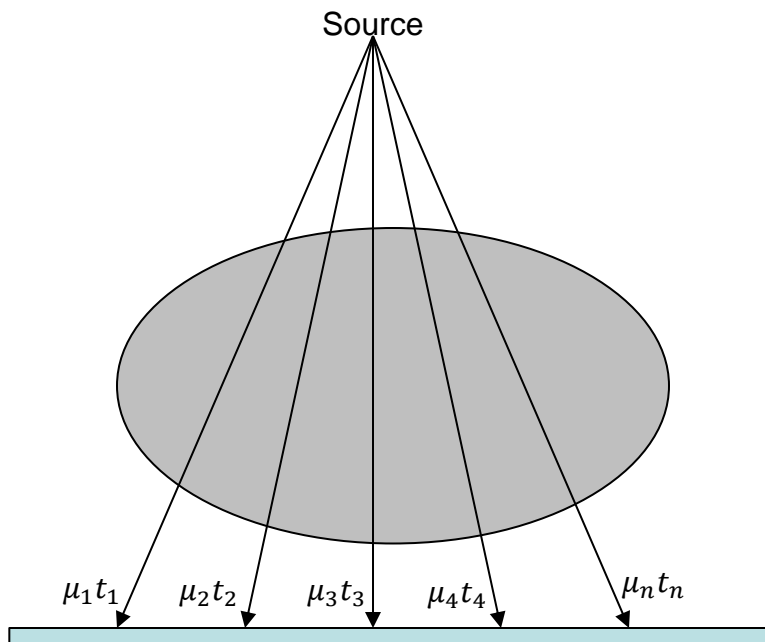
Crist BD, Khazzam M, Murtha YM, Della Rocca GJ: Pilon fractures: advances in surgical mgmt. J Am Acad Orthop Surg 2011; 19: 612-622

- Projected image can be thought of as the number of photons counted through each ray
  - Typically, the *darker* a section of the image is, the more photons were detected
    - Comes from the use of radiographic film where radiation would cause the film to darken
- Contrast
  - Refers to the ability to detect two different objects in an image
  - The larger the difference in attenuation between two objects (bone and tissue), the higher the contrast
    - Dependent on objects being measured, but also on the energy being used

I_0

μ_b	μ_b
μ_c	μ_a
μ_c	μ_b

t

$\mu_a < \mu_b < \mu_c$

$I_1 < I_2$

I_1 I_2
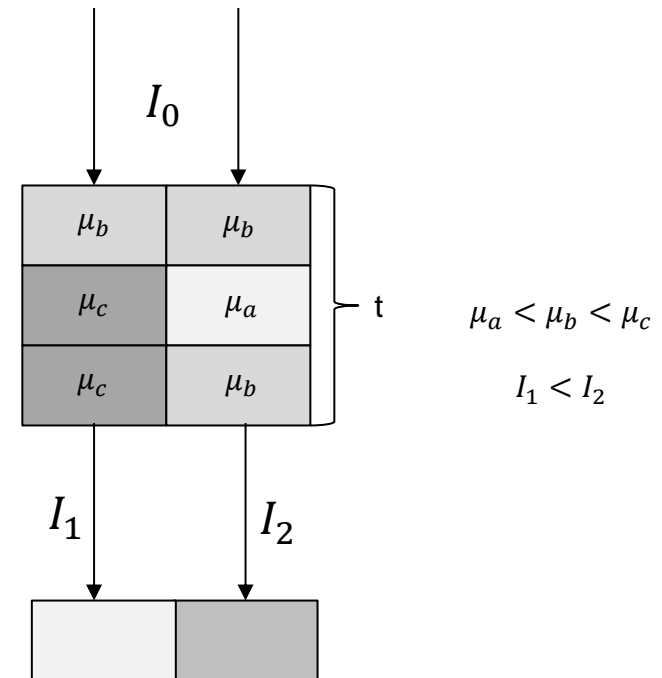
- Contrast of a system has two main dependencies
  - Patient anatomy
  - X-ray Spectrum
    - o Photoelectric Effect
      - Proportional to $\frac{Z^3}{E^3}$
      - At low energies, high density objects have a high contrast with their surroundings
    - o Compton Scattering
      - Proportional to electron per gram
      - Electrons per gram changes slowly with increasing Z
        - Amount of attenuation relies more on the density of material
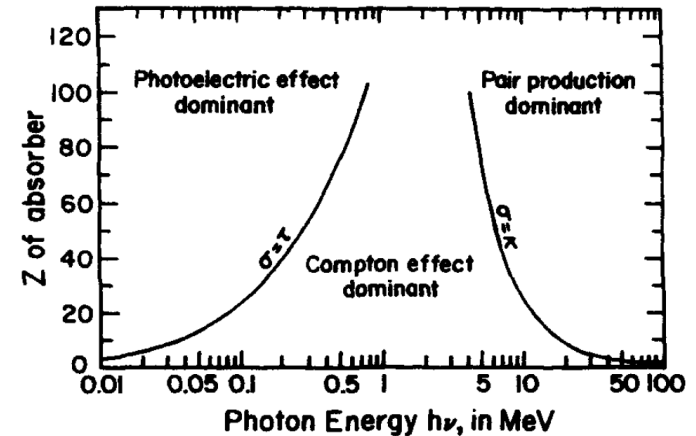
FH Attix. *Introduction to Radiological Physics and Radiation Dosimetry.* Wiley-VCH 2004
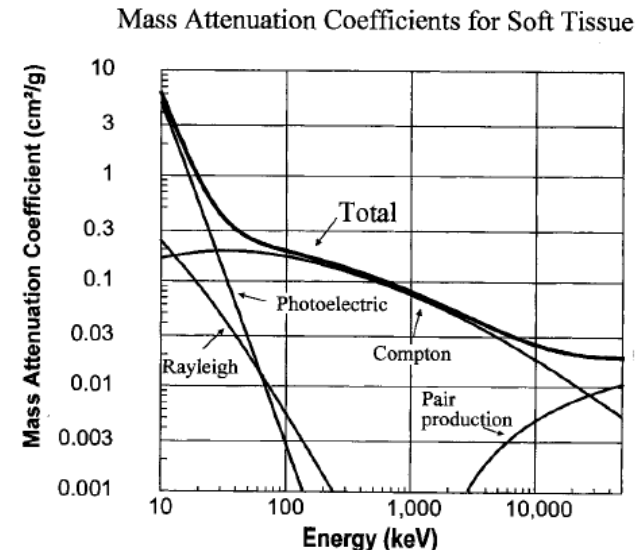
JT Bushberg, JA Anthony, EM Leidholdt, JR., JM Boon. *The Essential Physics of Medical Imaging.* Lipincott Williams & Wilkins, Philadelphia, USA 2002

- Basic X-Ray Tube
  - Electrons ejected from a Tungsten filament via thermionic emission
  - Electrons accelerated towards a tungsten target
  - Electrons strike target and produce photons via Bremsstrahlung
    - Electrons deflect in an electromagnetic field may lose energy via an emitted photon
    - Photons emitted nearly isotopically for low energy electrons
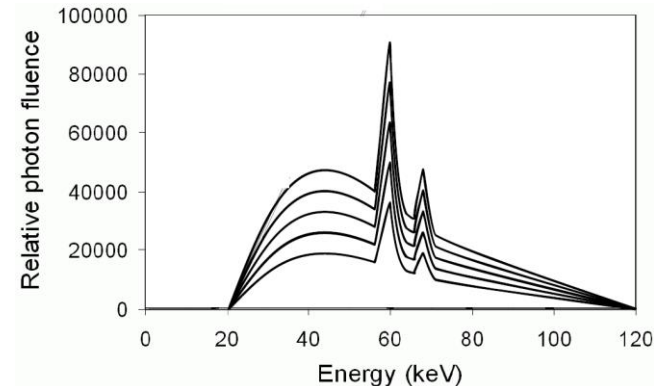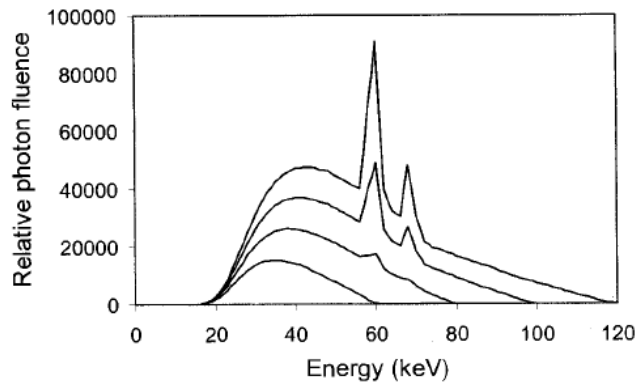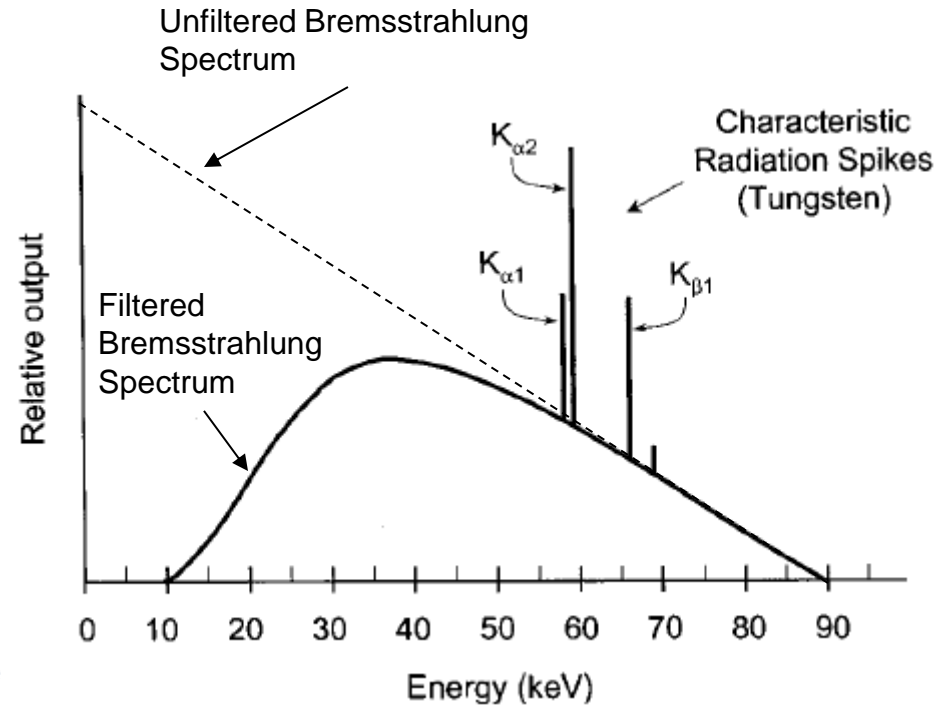   - $Efficiency = (9 \times 10^{-10})ZV$
  - Most of the energy is dissipated as heat
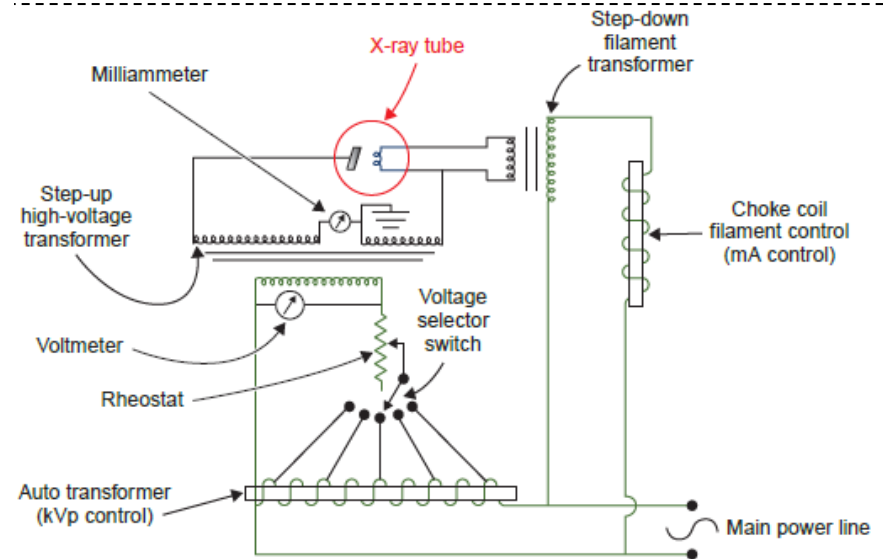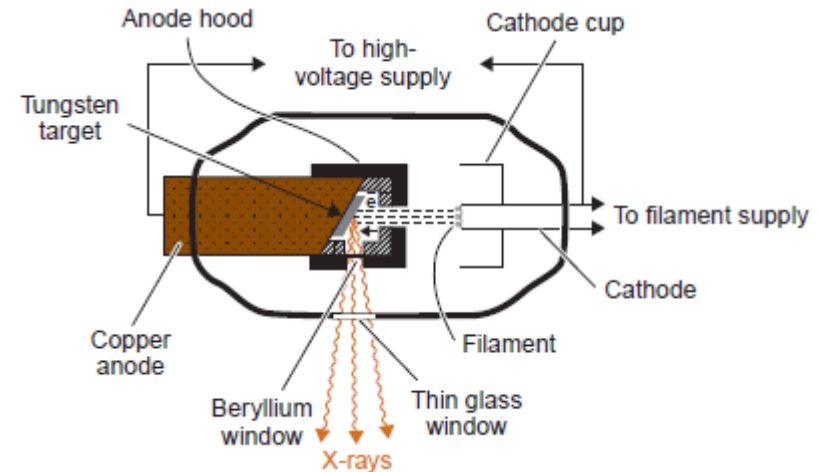
FM Khan and JP Gibbons. *Khan's The Physics of Radiation Therapy*. Fifth Edition Lippincott Williams & Wilkins, Philadelphia, USA 2014

- X-Ray Spectrum
  - Electrons can transfer any amount of energy, up to the energy of the electron, during Bremsstrahlung
  - Thin filters can be used to absorb the low energy photons
  - Number of photons varies the with tube current (mAs) and tube Voltage
    - Tube voltage also shifts the energy spectrum

Unfiltered Bremsstrahlung Spectrum

Characteristic Radiation Spikes (Tungsten)

$K_{\alpha2}$

$K_{\alpha1}$

$K_{\beta1}$

Filtered Bremsstrahlung Spectrum

Relative output

Energy (keV)

JT Bushberg, JA Anthony, EM Leidholdt, JR., JM Boon. *The Essential Physics of Medical Imaging.* Lipincott Williams & Wilkins, Philadelphia, USA 2002

- X-Ray Detectors
  - X-rays strike a scintillator and generate optical light
    - Scintillator is designed in an array segmented by reflectors
      - Reflectors prevent light escaping each scintillator component
  - Optical light is absorbed by a photodiode layer where it is converted into an electrical signal
    - 1 photodiode per scintillator segment
    - Signal is proportional to the light intensity
  - A substrate is used to provide the mechanical and electrical infrastructure of the device

X-Rays

Scintillator

Photodiode

Substrate

Signal

Top View

Z-Axis
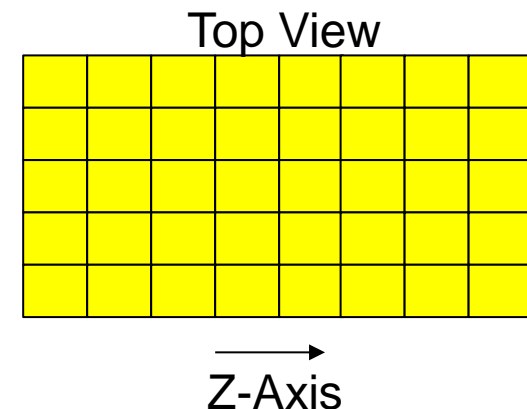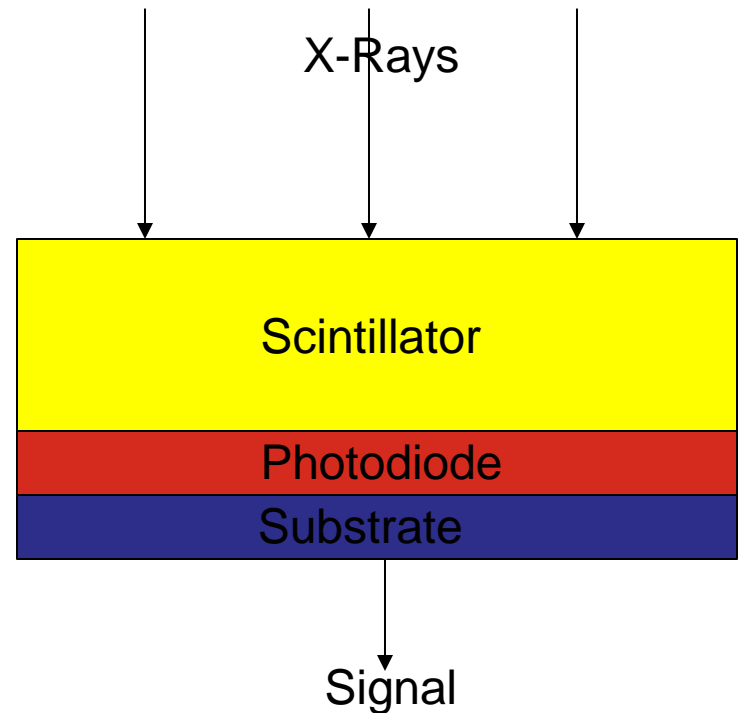
- Detector Characteristics
  - Scintillators (Single Crystals and Polycrystaline Ceramics)
    - High light output
    - High Stopping Power
    - Short decay time
    - Low afterglow
    - Compact packaging and cost effect production
  - Photodiode Arrays (Back-illuminated PDA)
    - High responsivity (100% Quantum Efficiency)
    - High shunt resistance
    - Minimal crosstalk
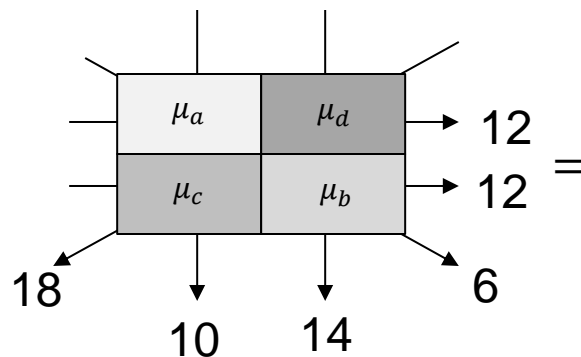   - High linearity
    - Fast response time

Fig. 10 Garnet-type (*left*), Gd$_2$O$_2$S:Pr,Ce (*center*), and ZnSe (*right*). Scintillator wafers (photo courtesy Philips Healthcare)
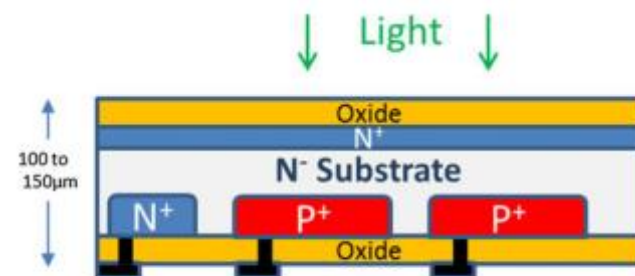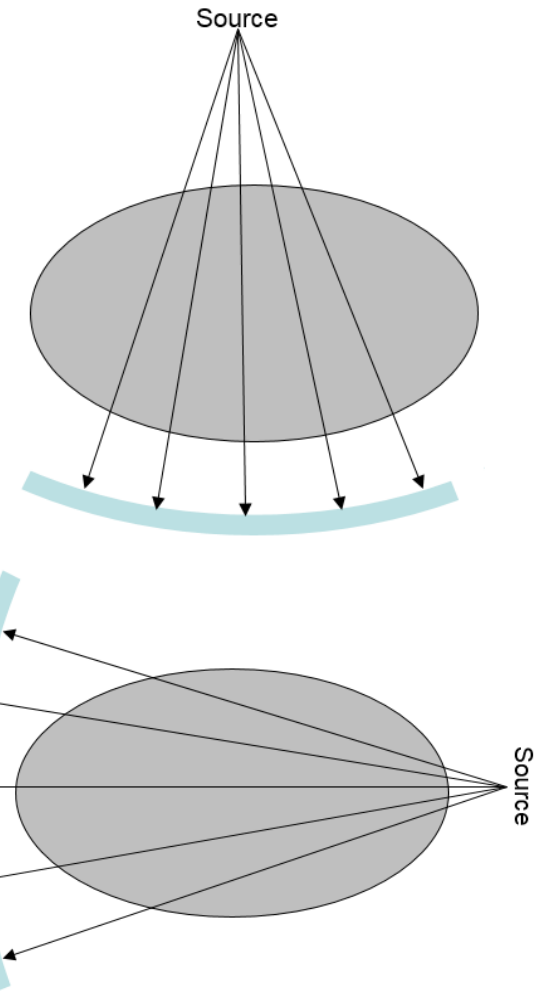
Fig. 12 Back-illuminated PDA. The PDA is illuminated from one side, while the electrical contacts and the junctions are on the other side. The overall thickness is in the order of 100–150 μm

E Shefer et. al. "State of the Art of CT Detectors and Sources: A Literature Review: Curr Radiol Rep (2013) 1:76-91

- Computed Tomography
  - CT acquires multiple projections at different angles
  - Each projection image can be stored in Radon space
    - All projections make-up sinogram space
  - In practice, each projection at every angle is back-projected to determine the attenuation at each voxel

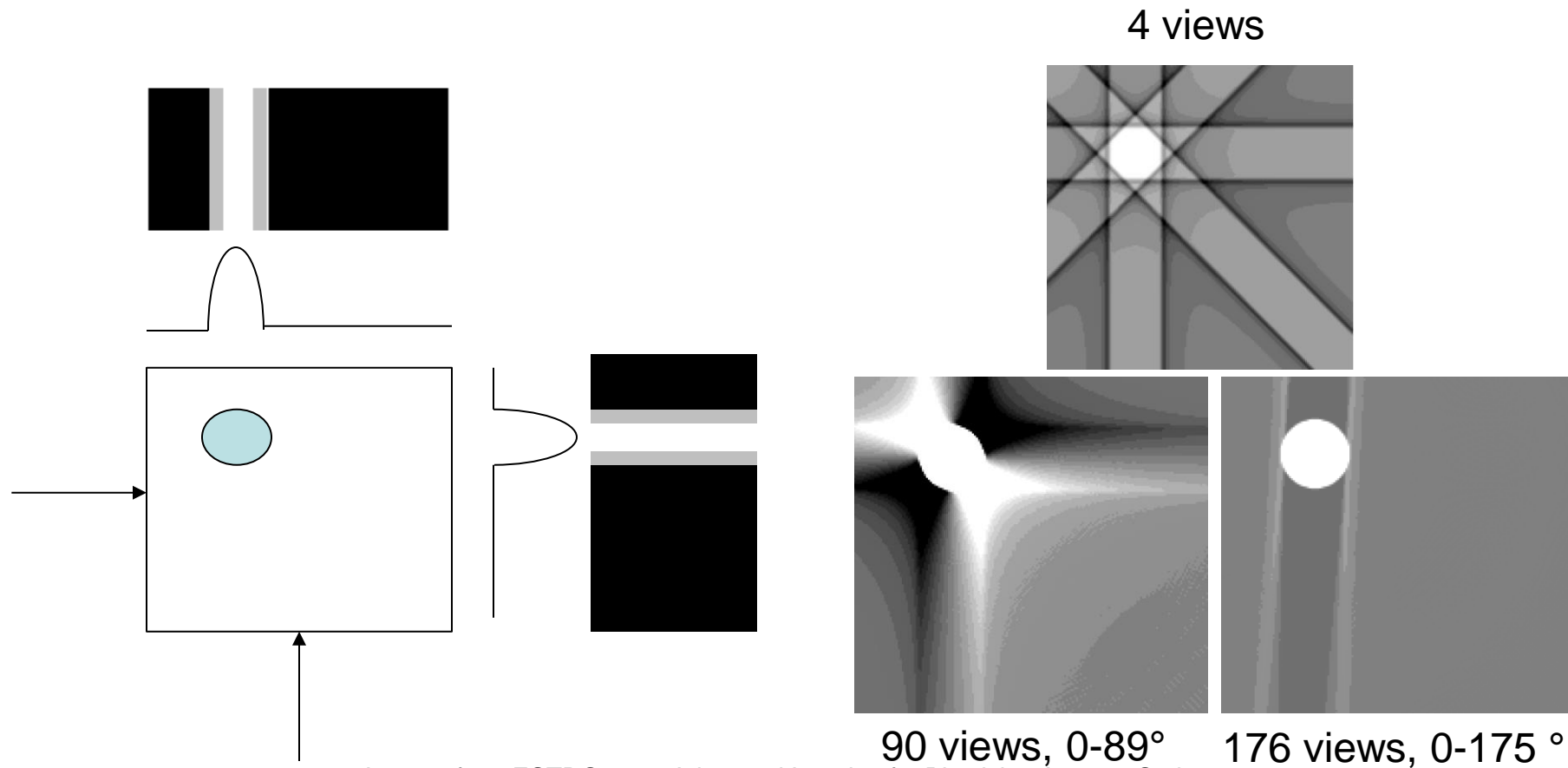Linear Space

S

Radon Space

θ

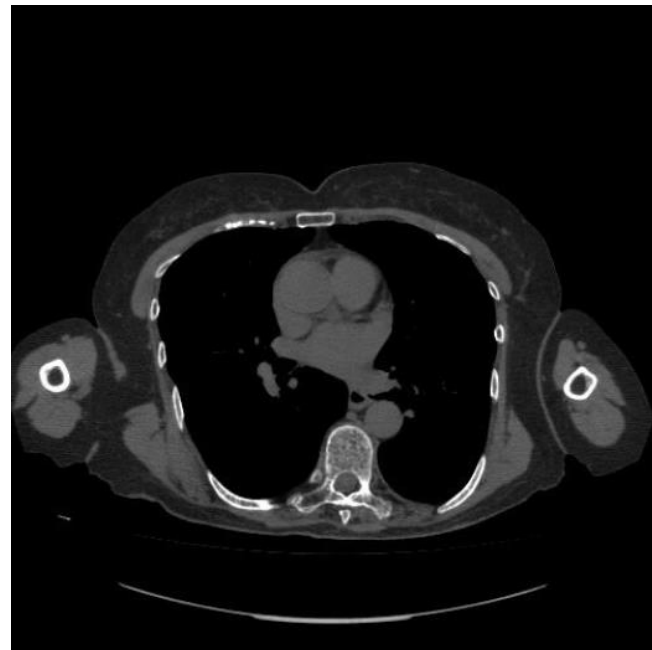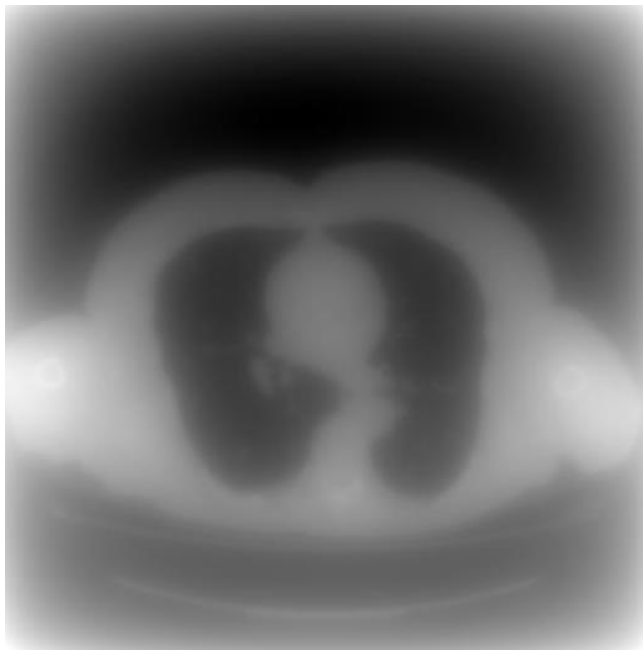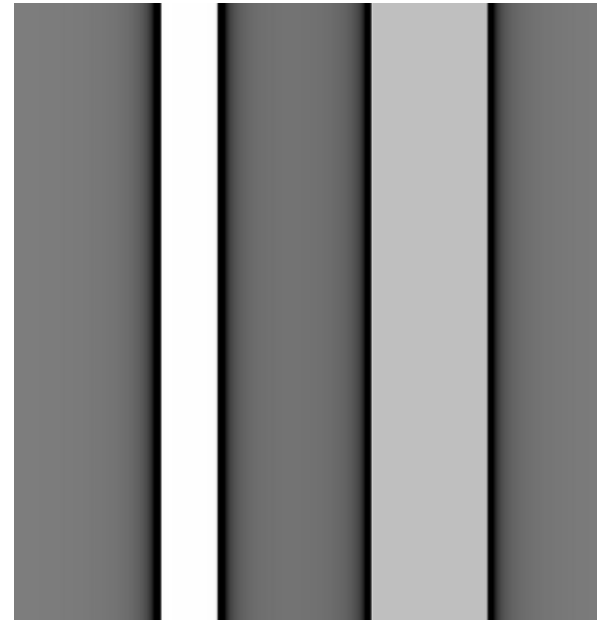Images from ESTRO 2013 Advanced Imaging for Physicists Lecture Series
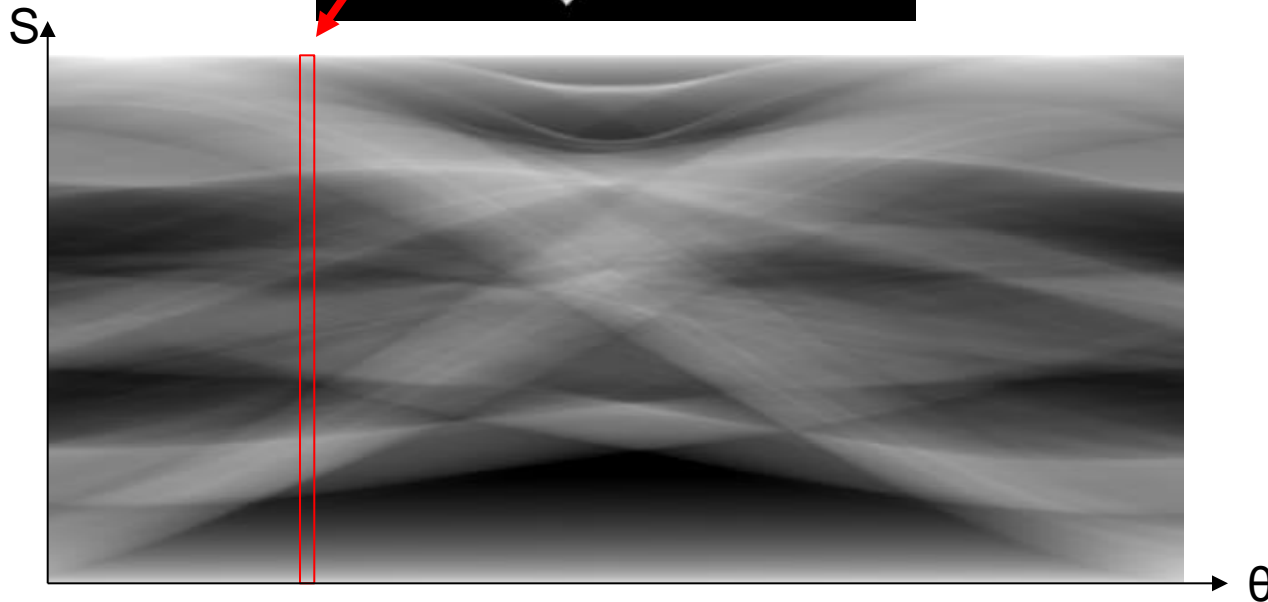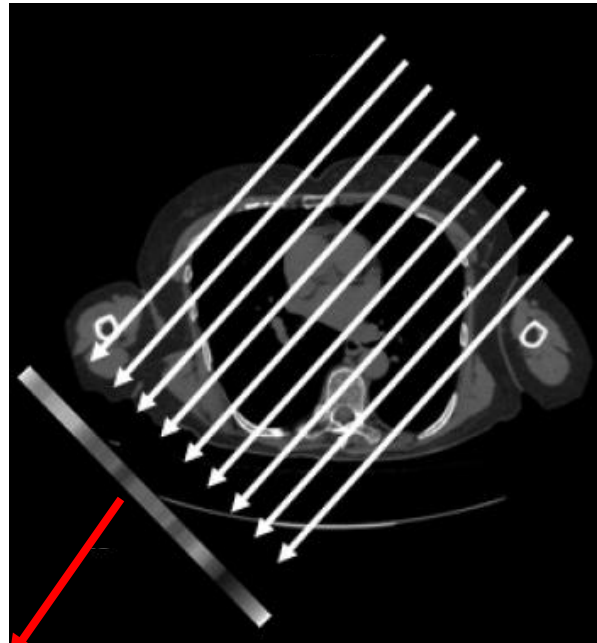
- 1D Fourier transform of each projection image in Radon Space yields an angulated line is Fourier Space

  - 2D Fourier transform of Linear Space also results in a 2D Fourier Space

- Basic image reconstruction algorithm

  - Acquire projection images to develop Radon Space
  - Perform 1D Fourier Transform to develop Fourier Space
  - Apply filters in Fourier Space
  - Perform inverse 1D Fourier Transform to develop filtered Radon Space
  - Perform back projection to develop image in linear space

1D Fourier Transform

Images from ESTRO 2013 Advanced Imaging for Physicists Lecture Series
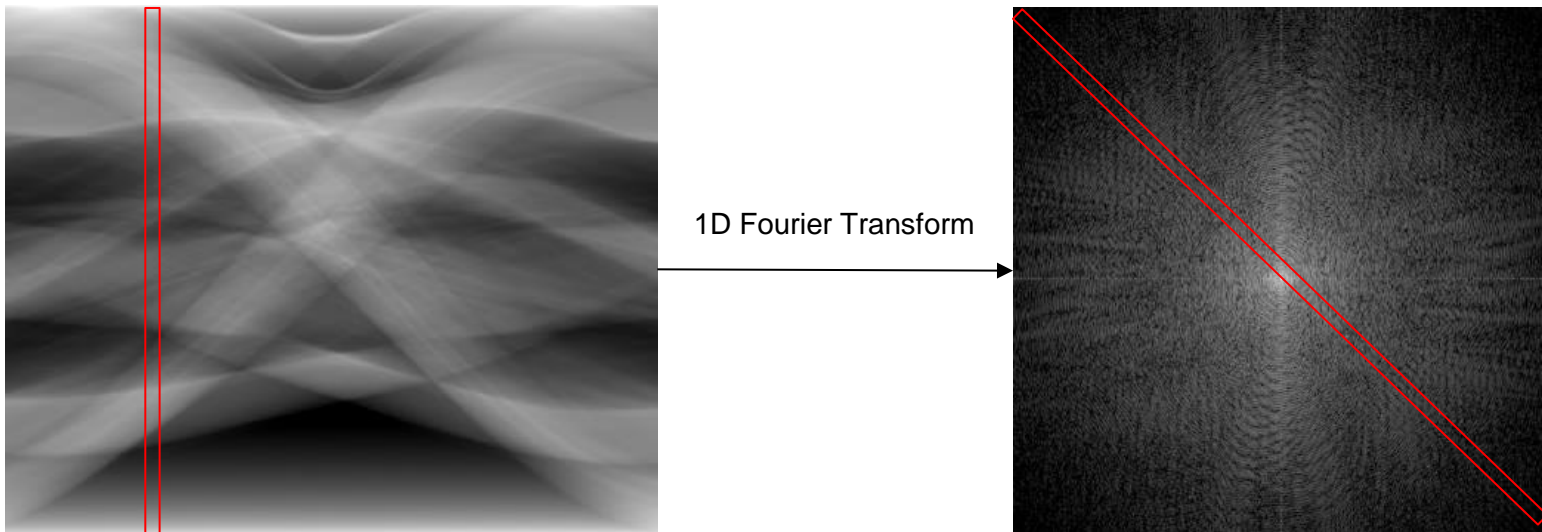
- Back Projection
  - Each measurement in a projection is projected back into the image along each ray
  - At each point, projection images are overlayed and measured signals are combined

4 views

90 views, 0-89°   176 views, 0-175 °

Images from ESTRO 2013 Advanced Imaging for Physicists Lecture Series
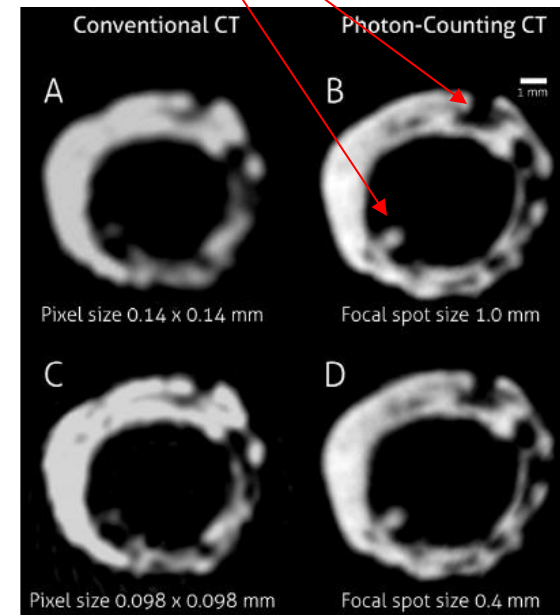
Images from ESTRO 2013 Advanced Imaging for Physicists Lecture Series

- Photon Counting CT Systems
  - Conventional CT detectors measure integrated energy at the detector
  - Photon Counting detectors detect individual photons and measure their energy
    - Allows for dose reduction, increased spatial resolution, correction of beam-hardening, alternative contrast agents
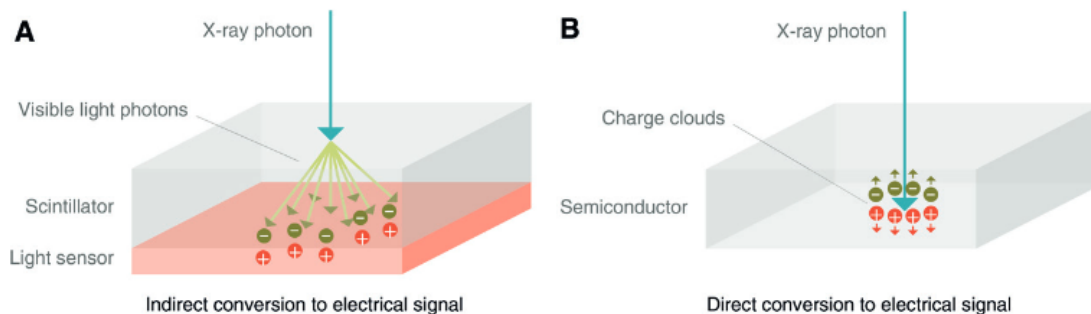
Figure 1: Diagrams show detector types. A, In conventional energy-integrating detector, an incident x-ray photon is converted into a shower of visible light photons in a scintillator. Visible light hits an underlying light sensor, where it generates positive and negative electrical charges. B, In photon-counting detector, the x-ray photon is absorbed in a semiconductor material, where it generates positive and negative charges. Under the influence of a strong electric field, the positive and negative charges are pulled in opposite directions, generating an electrical signal.

MJ Willemink et. al. "Photon-counting CT: Technical Principles and Clinical Prospects". Radiology 289:2; 293-312 (2018)

- Artificial Intelligence
  - AI algorithms are becoming a critical tool in image analysis
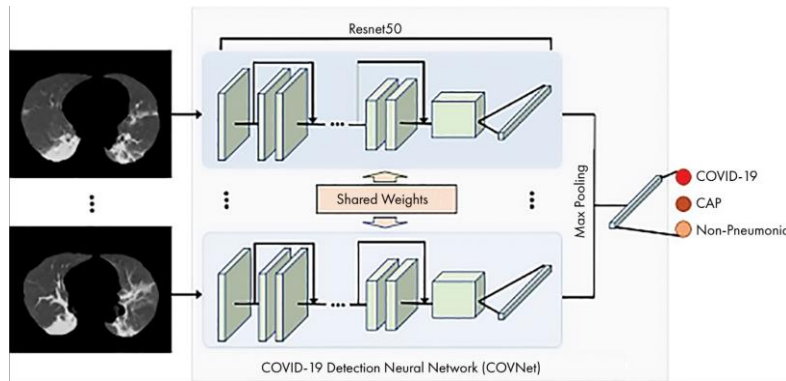   - Segmentation, early cancer detection, diagnosis, etc.

Using Artificial Intelligence to Detect COVID-19 and Community-acquired Pneumonia Based on Pulmonary CT: Evaluation of the Diagnostic Accuracy

Lin Li, BS • Lixin Qin, PhD • Zeguo Xu, BS • Youbing Yin, PhD • Xin Wang, PhD • Bin Kong, PhD • Junjie Bai, PhD • Yi Lu, MS • Zhenghan Fang, MS • Qi Song, PhD • Kunlin Cao, PhD • Daliang Liu, PhD • Guisheng Wang, PhD • Qizhong Xu, MS • Xisheng Fang, BS • Shiqin Zhang, BS • Juan Xia, BS • Jun Xia, PhD

Table 3: Performance of Deep Learning Framework COVNet on the Independent Testing Set

Group	Sensitivity (%)	Specificity (%)	AUC	P Value
COVID-19	90 (114 of 127) [83, 94]	96 (294 of 307) [93, 98]	0.96 [0.94, 0.99]	<.001
CAP	87 (152 of 175) [81, 91]	92 (239 of 259) [88, 95]	0.95 [0.93, 0.97]	<.001
Non-pneumonia	94 (124 of 132) [88, 97]	96 (291 of 302) [94, 98]	0.98 [0.97, 0.99]	<.001

Note.—Values in parentheses are the numbers of scans for the percentage calculation. Values in brackets are 95% confidence intervals. AUC = area under the receiver operating characteristic curve, CAP = community-acquired pneumonia, COVID-19 = coronavirus disease 2019, COVNet = COVID-19 detection neural network.
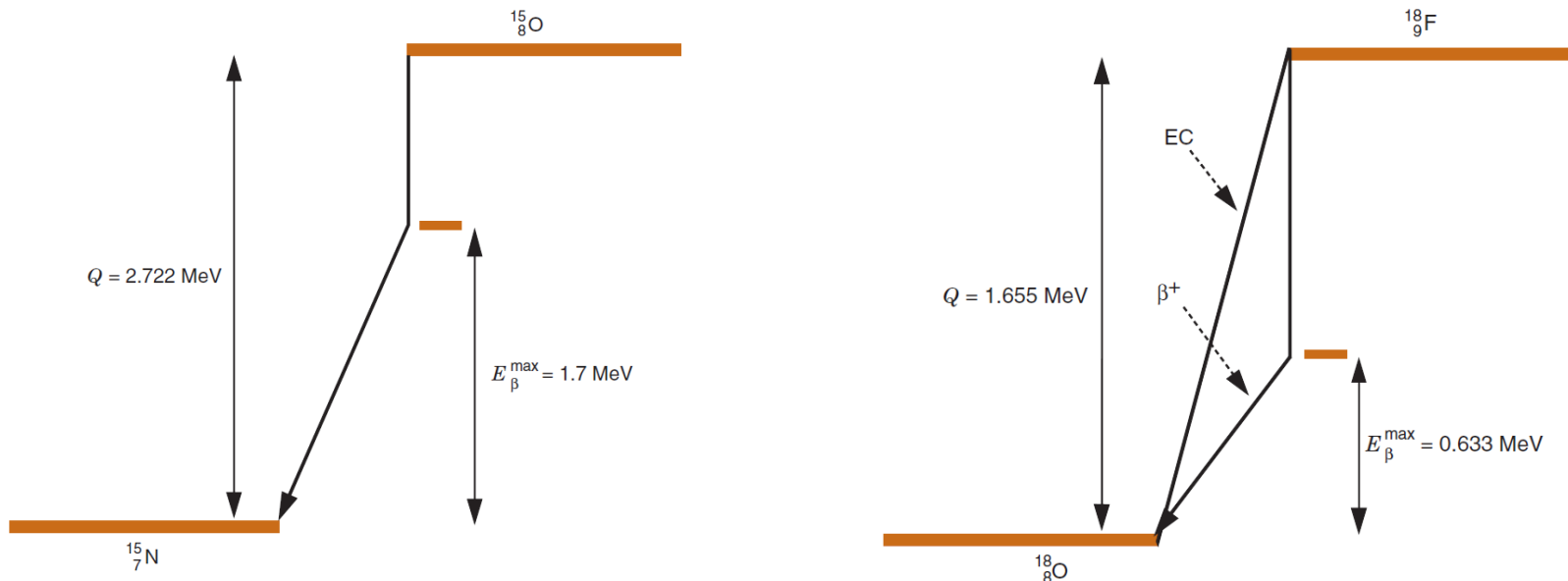
L Li et. al. "Using Artificial Intelligence to Detect COVID-19 and Community-acquired Pneumonia Based on Pulmonary CT: Evaluation of the Diagnostic Accuracy" Radiology 296:2; E65-E71

Positron Emission Tomography

- PET Basics
  - Utilizes positron emitting radioisotopes
    - Radioisotopes attached to a "tracer" which can be targeted to a specific function
  - Measured data are a result of positron annihilation
  - Detectors typically consist of a grid of scintillating crystals and photomultiplier tubes
  - If the signal generated in two separate PMTs falls within a specific coincidence window, a Line of Response can be drawn between the two detection sites
    - Specifies the probability that the decay occurred somewhere along that line
  - Over many Lines of Response an image can be reconstructed
  - PET images are most commonly used in Oncology
    - Target Delineation
   - Staging
    - Functional Status

- β⁺ Decay

$$_{Z}^{A}X \rightarrow {}_{Z-1}^{A}Y + \beta^{+} + \nu + Q$$

  - "Conversion" of a proton to a neutron and positron
    - Neutrino and excess energy released in the process
  - Occurs in light nuclei that have a deficit of neutrons
    - n/p ratio is lower than that of stable nuclei
    - Decay mode must increase the n/p ratio

SR Cherry, JA Sorenson, ME Phelps. "Physics in Nuclear Medicine" Philadelphia, PA. Elsevier Saunders 2012
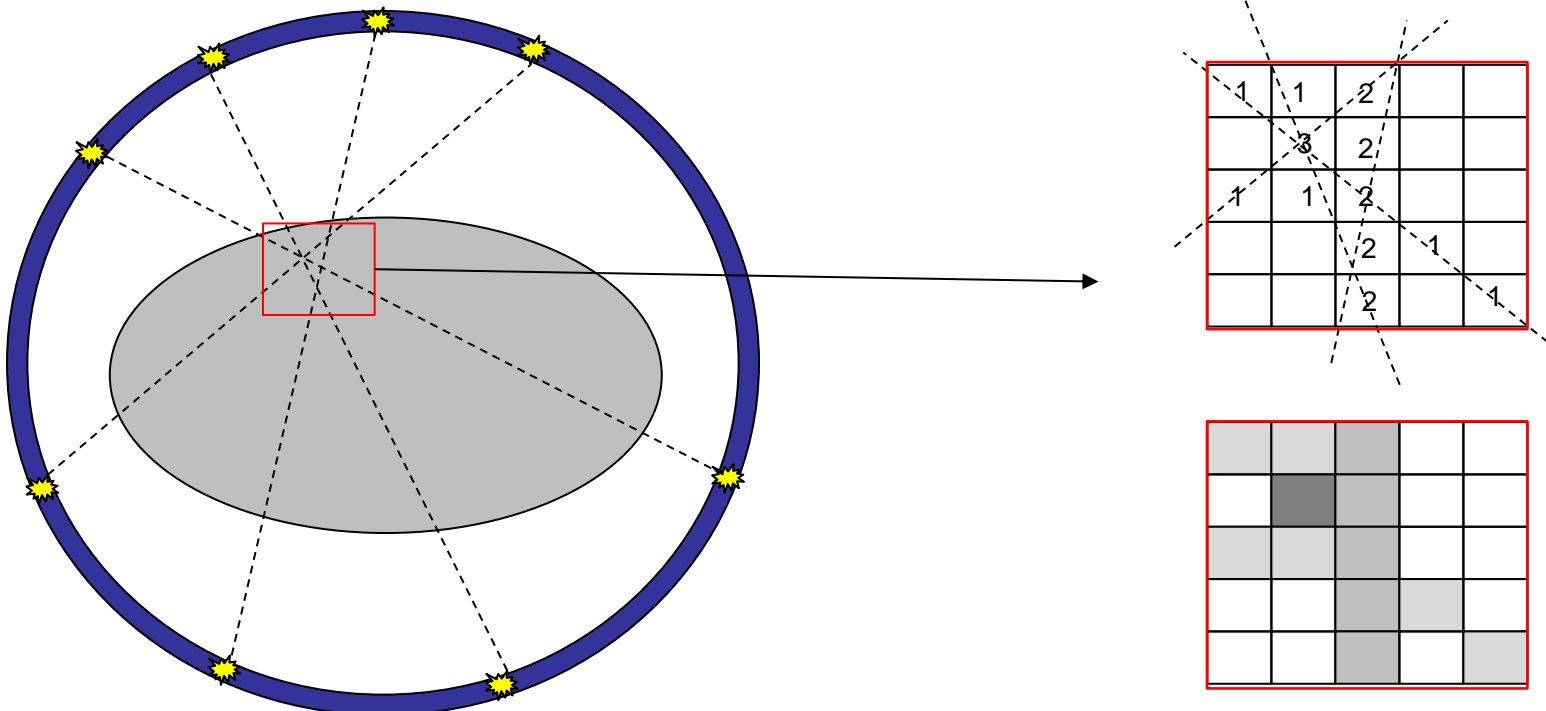
- Positron Annihilation
    - After the beta decay, the positron may travel a small distance from the nucleus
        - Minimum energy of 1.022 MeV
        - Interacts and loses energy similar to an electron
    - Once the positron has lost its kinetic energy, it will interact with an electron in an annihilation event
    - Result of annihilation is two photons, each with an energy of 0.511 MeV
        - Photon energy is equivalent to the rest mass of an electron
        - Photons are emitted in *nearly* opposite direction
            - A small amount of momentum from the positron must be conserved, results photon emission slight less than 180°

γ

~180°

β⁺   e⁻

γ
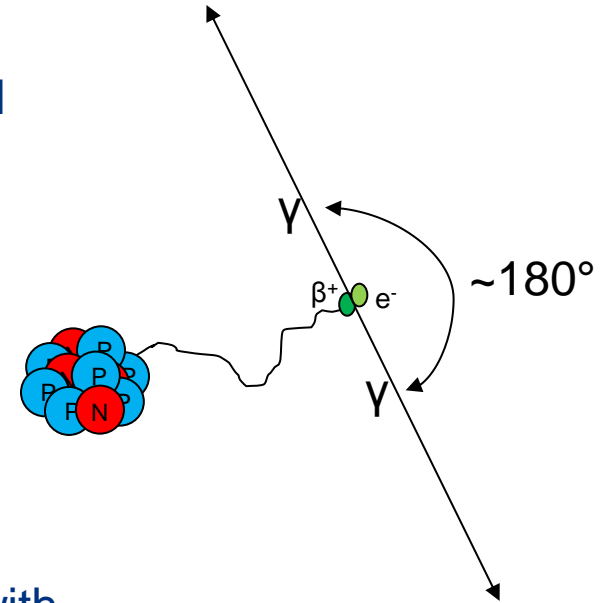
- PET takes advantage of the annihilation photons to determine the origin of the positron
  - The positron moves only a small distance away from the originating nucleus, can be assumed the annihilation event is local to the decay event
    - Max range of a positron from F-18 decay is 2.6mm
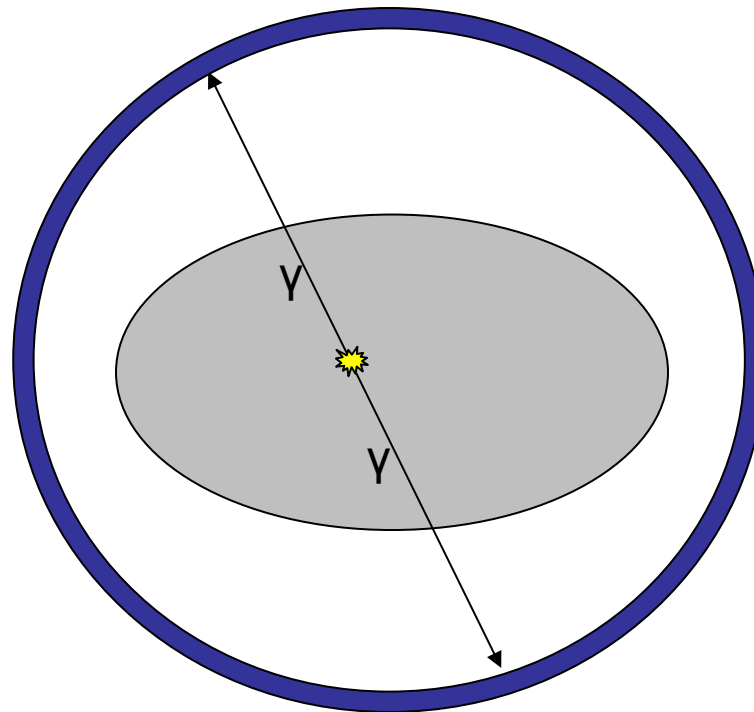
- For each photon pair detected, a line-of-response (LOR) can be drawn between the detection sites

  - Photon must be detected within a specified detection window

  - Without any corrections, the annihilation event has an equal probability of occurring anywhere along the LOR

  - Over a large number of detections, the intersection of those LORs identifies the location of the annihilation event

- Gamma Detection
  - Annihilation Photon interacts in a scintillating crystal
  - Photons generated in the scintillating crystals enter a series of Photomultiplier Tubes (PMTs)
  - PMTs convert the scintillating photons to an electrical signal
 - Signals read out by PET circuitry to determine timing and position

Top View

Side View

Scintillating Crystals

PMTs
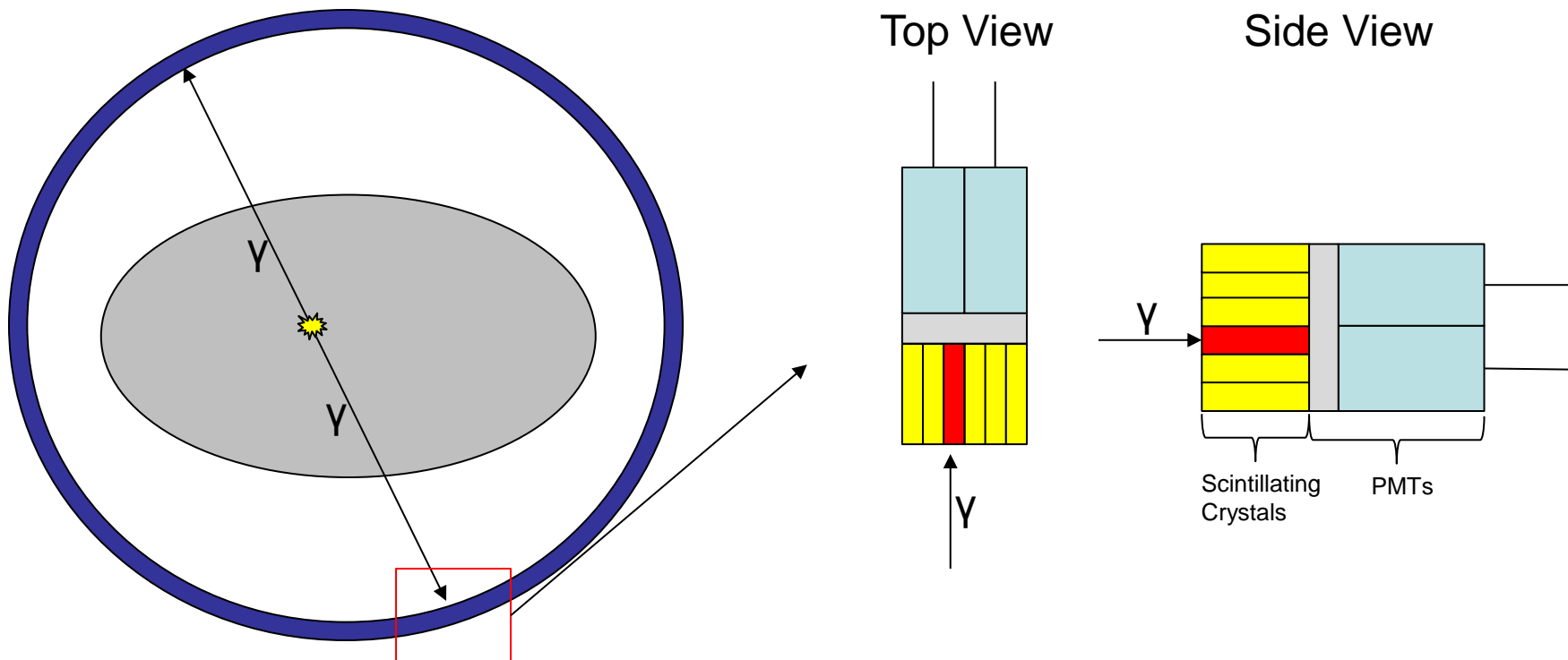
- Scintillating Crystals
  - Incident photon will create an energetic electron in the scintillator
    - Photoelectric Effect $\left(\propto \frac{Z^3}{E^3} \right)$
    - Energetic electron will transfer it's energy to other electrons as it travels through the scintillator, elevating them to an excited state
  - Excited electrons will degrade to their ground state, emitting a photon
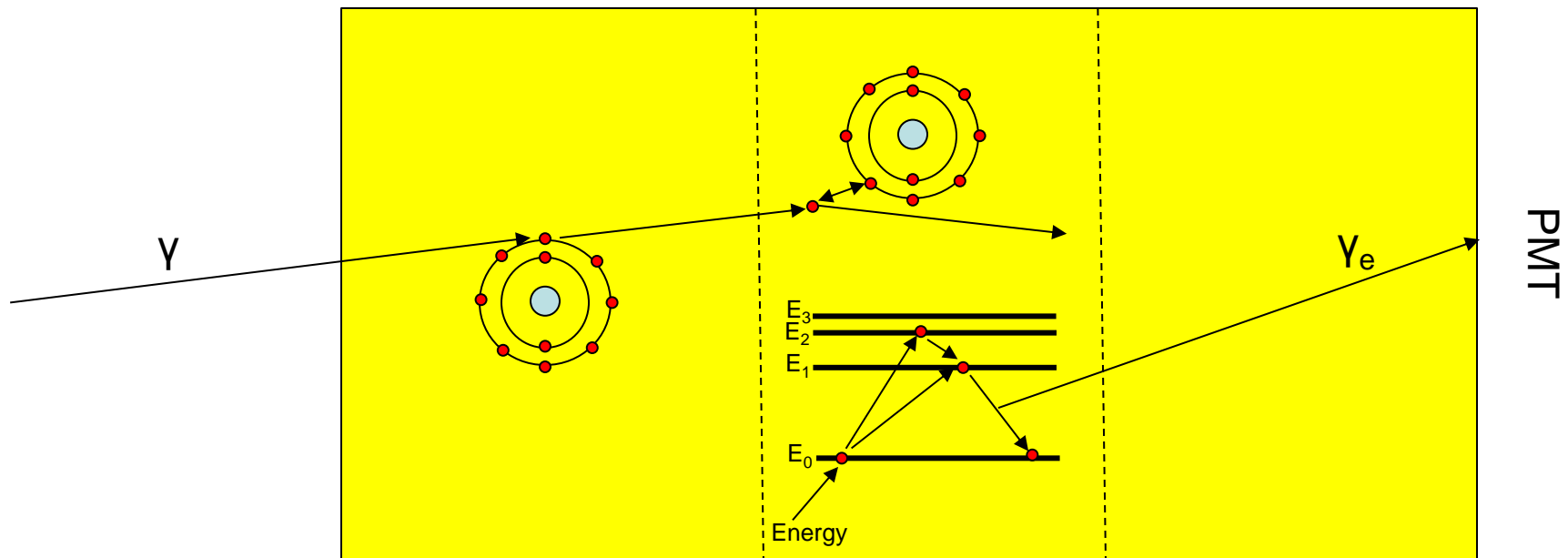
- Scintillating Crystals Characteristics

  - High Stopping Power (μ)

    - Increases sensitivity
    - Increases spatial resolution

  - High Light Output

    - Increases energy resolution
    - Increases spatial resolution

  - Fast Decay (τ)

    - Decreases dead-time
    - Increases timing resolution

- Common Scintillators

  - Sodium Iodide (NaI)

  - Bismuth Germanate (BGO)

  - Cerium-doped Lutetium Oxy-Orthosilicate (LSO)

|	1970's	1980's	2000's
Scintillaor	NaI	BGO	LSO/LYSO
μ (cm^{-1})	0.35	0.95	0.86
Output (% NaI)	100	15	70
τ (ns)	230	300	40

- Photomultiplier Tubes
  - Emitted photon from scintillator strikes a photocathode, converting the photon to an electron
  - Electron is accelerated through a series of dynodes
    - Electrons strike each dynode and, through secondary emission, generate additional electrons
  - Electrons are collected at the anode, generating an electrical pulse proportional to the number of electrons present
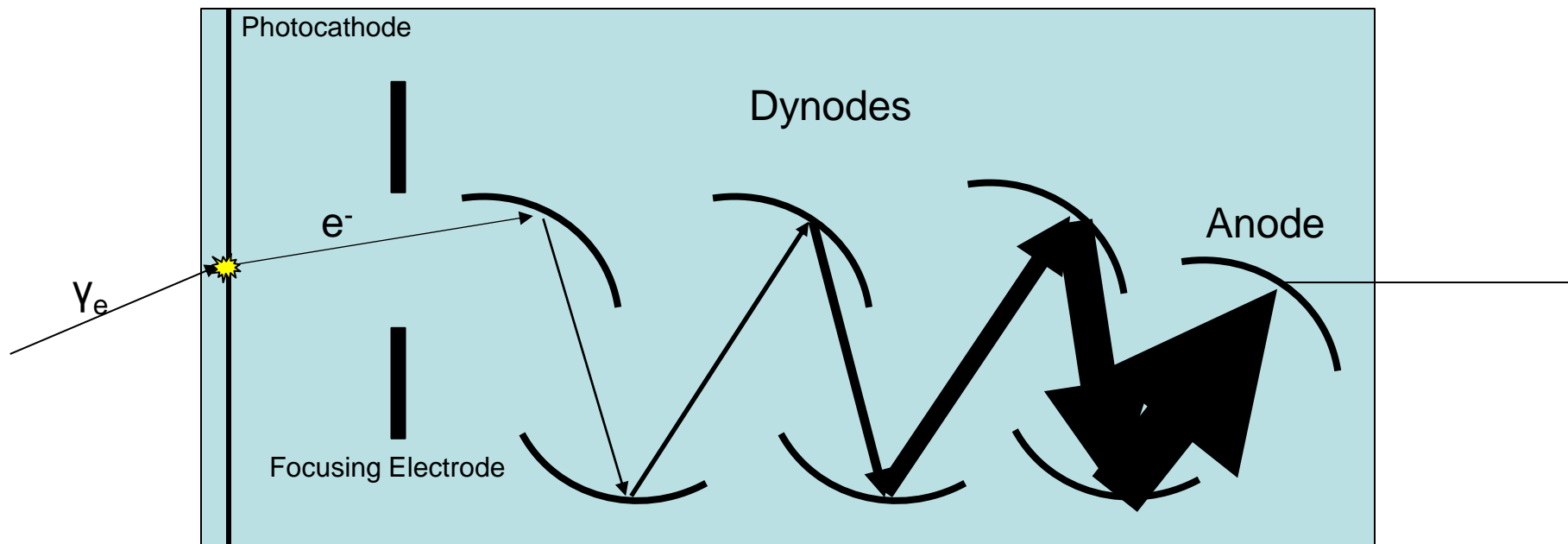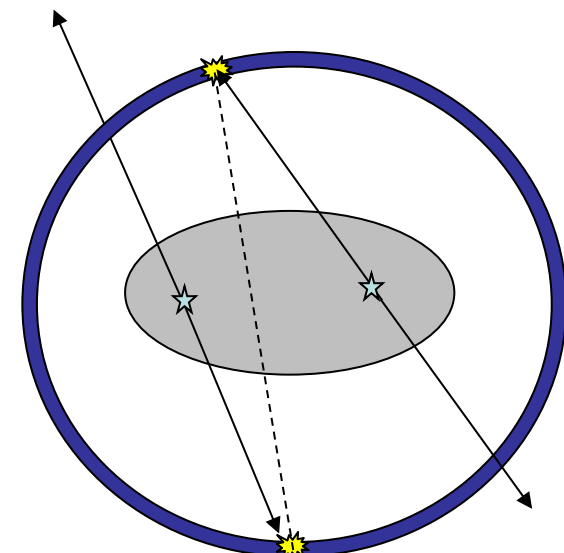
- Ideally, the LOR would pass through the point of origin
  - True Coincidences
    - Both photons from the same annihilation event are detected within the coincidence window
  - Scatter Coincidences
    - One of the annihilation photons is scattered before being detected
    - Also a True Coincidence, but provides incorrect spatial information
  - Random Coincidences
    - Two annihilation photons from different annihilation events are detected inside the coincidence window
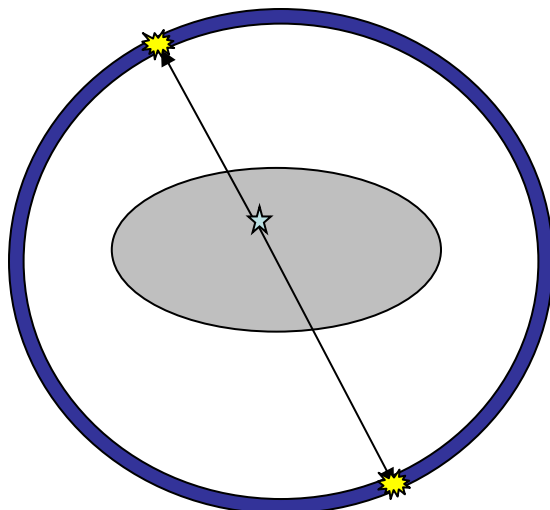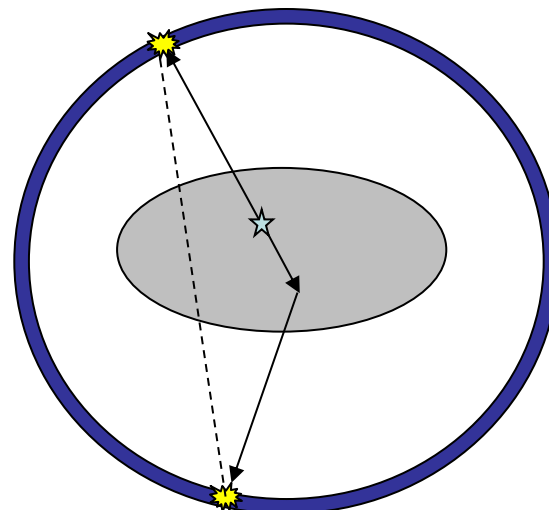
True Coincidence   Scatter Coincidence   Random Coincidence

- Timing Detection
  - Pre-determined coincidence window must be defined
    - Window starts on the leading edge of signal from the PMT
  - Window width must account for photon travel time within the detector, but mainly characteristics of the detector system
    - Typical window width on the order of ~10^{-9} sec

Signal A

Coincidence Window

Signal B

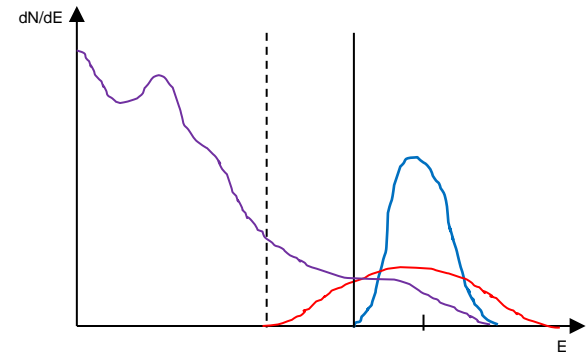Coincidence   No Coincidence   Coincidence
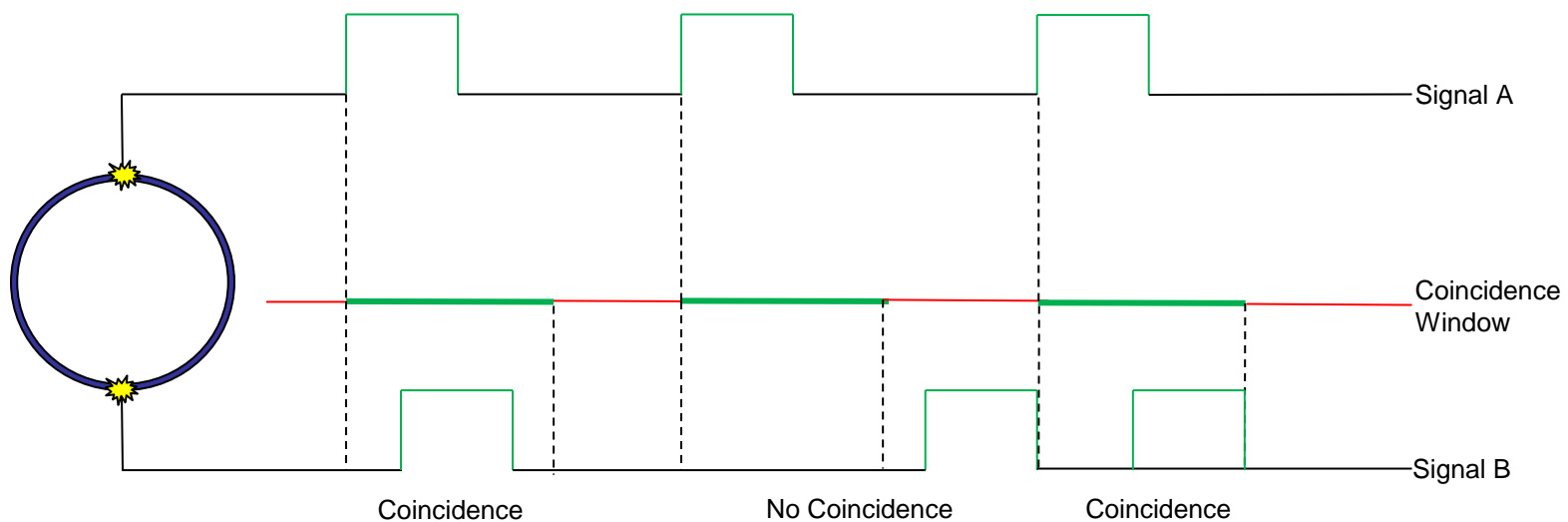
- Energy Discrimination
  - High energy resolution can assist in filtering out scatter detections
  - Monoenergetic annihilation photons result in a narrow energy distribution of electrons in the scintillator
    - This energy distribution is blurred based on the energy resolution of the system
  - High energy resolution systems can assist in filtering out lower energy scattered photons
    - Some scatter will still remain, which results in more image noise
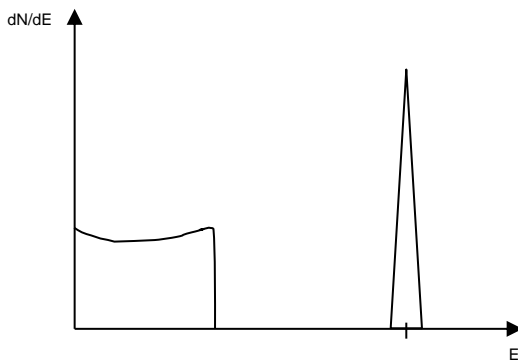
Energy distribution for an ideal scintillator system exposed to monoenergetic photons
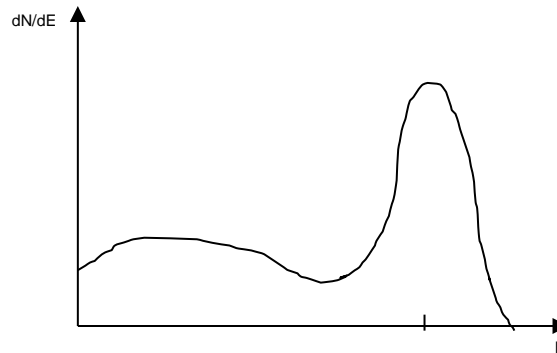
Energy distribution for realistic scintillator system exposed to monoenergetic photons

Energy distribution for True coincidences in a high energy resolution system (blue), True coincidences in a low energy resolution system (red) red), and Scatter (purple), coincidences in a PET system
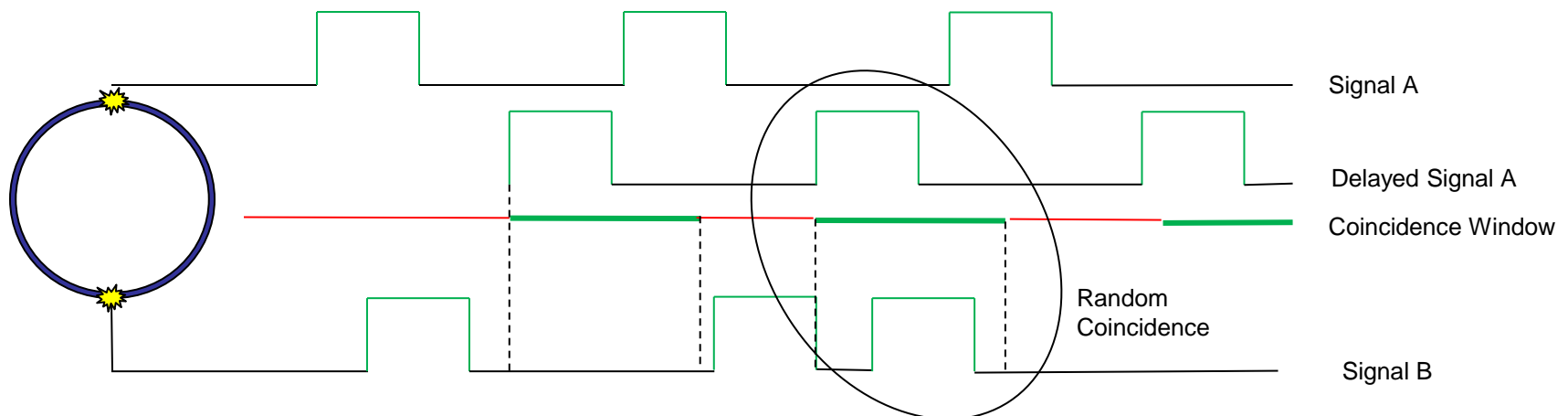
- Random Coincidences
  - The rate of random coincidences between any two pairs of detectors is modeled as

  $$R_{random} = 2\tau S_1 S_2$$

  where τ is the coincidence window and S_1 and S_2 are the detector count rates
  - Ratio of random to true coincidences increases with increased administered activity and decreases with a shortened coincidence window
    - Minimum coincidence window is determined by the detector system
  - The number of random coincidences along a lie of response can be measured using a delayed window technique
    - Cannot tell which detections are random, only the amount of randoms detected

Signal A

Delayed Signal A

Coincidence Window

Random Coincidence

Signal B

- Scatter Coincidences
  - Fraction of scatter coincidences is independent of administered activity or the coincidence window
  - Better energy resolution can remove some scatter, but not all
  - Scatter is variable based on the patient size
    - Larger patients result in more scatter coincidences
  - Model-based scatter correction algorithms are typically employed to reduce scatter
    - Many algorithms based on the Klein-Nishina formula to determine a representative percentage of scattered photons

$$\frac{d\sigma}{d\Omega} = \frac{Zr_0^2}{2}\left(1 + (E/m_0c^2)(1 - cos\theta)\right)^{-2}(1 + cos^2\theta)\left(1 + \frac{(E/m_0c^2)^2(1 - cos\theta)^2}{(1 + cos^2\theta)\left(1 + (E/m_0c^2)(1 - cos\theta)\right)}\right)$$

- Number of other Corrections useful in PET
  - Attenuation correction
    - Utilizes attenuation information from a transmission scan or CT to correct for energy loss and attenuation as photons travel through a patient
  - Time-of-Flight
    - Differences between detections in a true coincidence can be used to narrow probability of where on a LOR the emission occurred
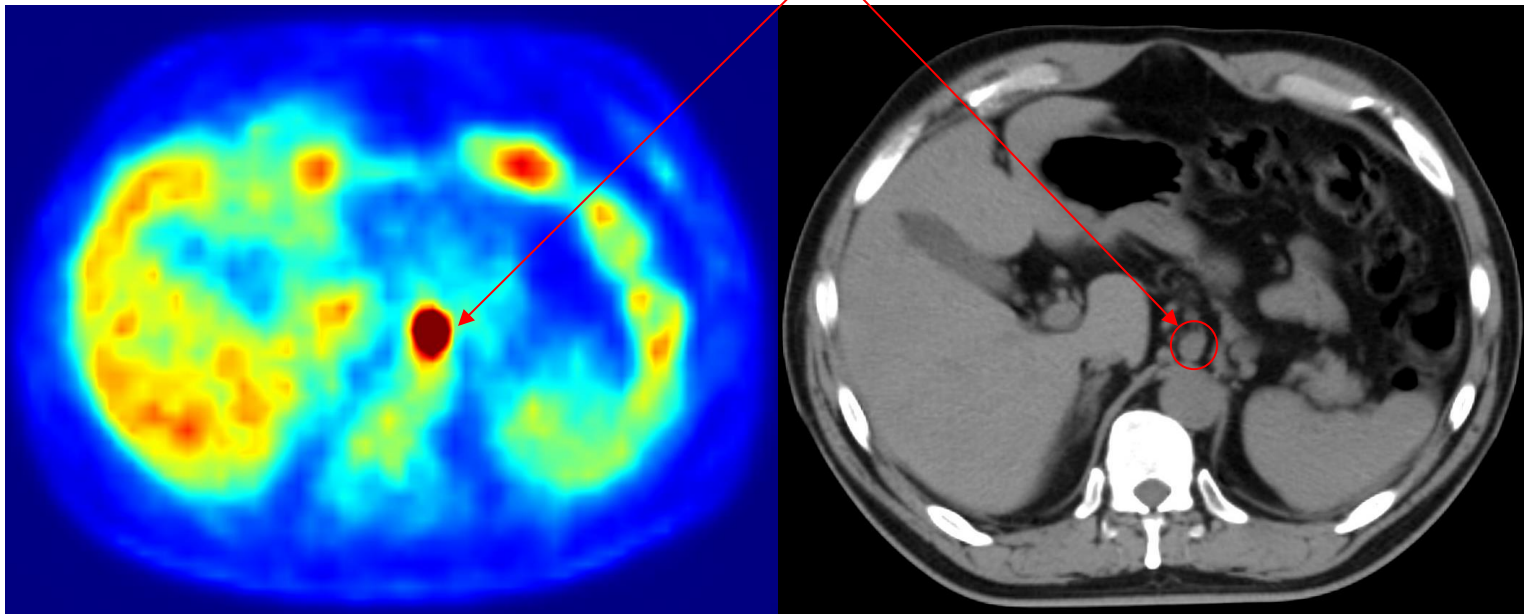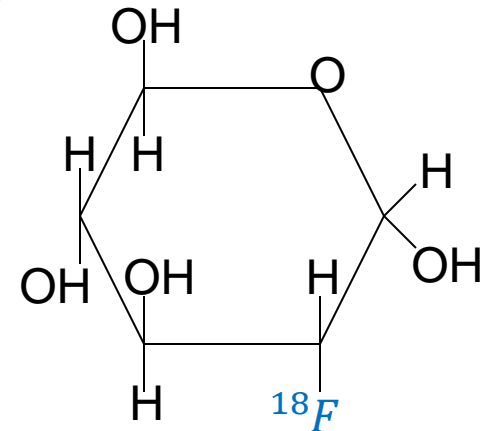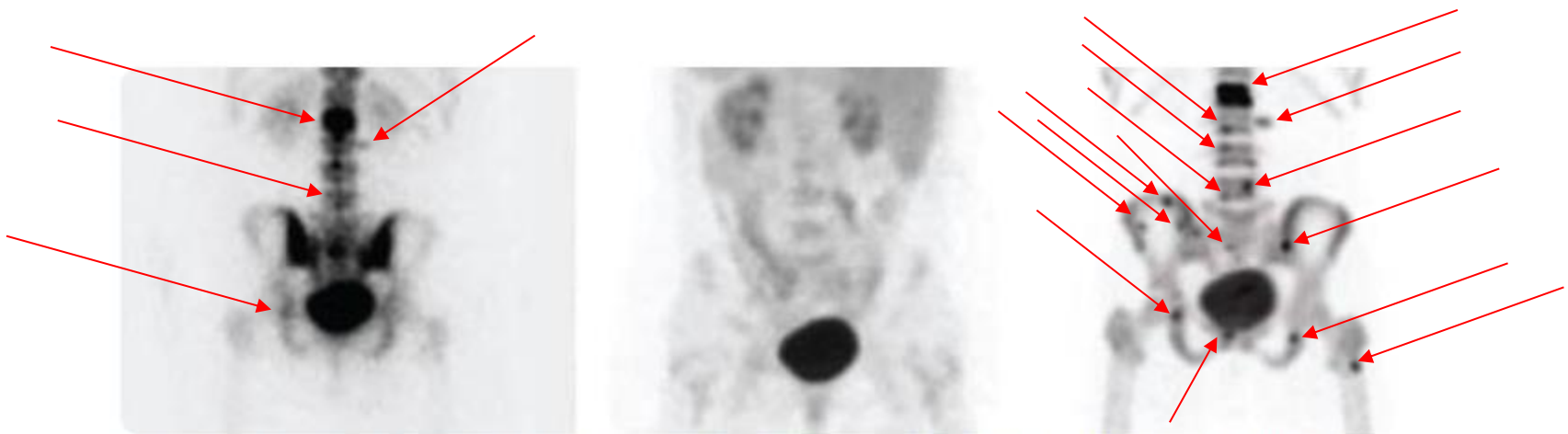
No Attenuation Correction
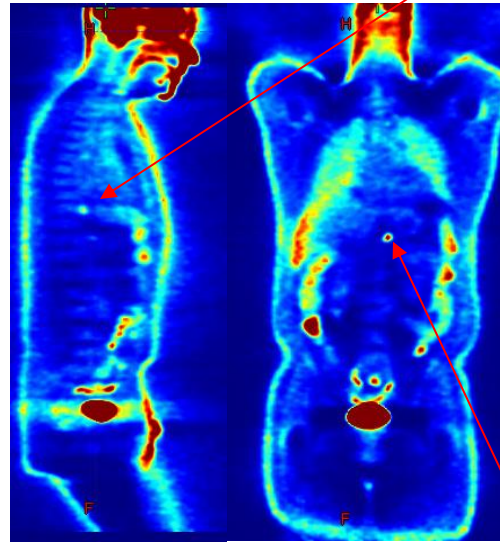
Attenuation Correction
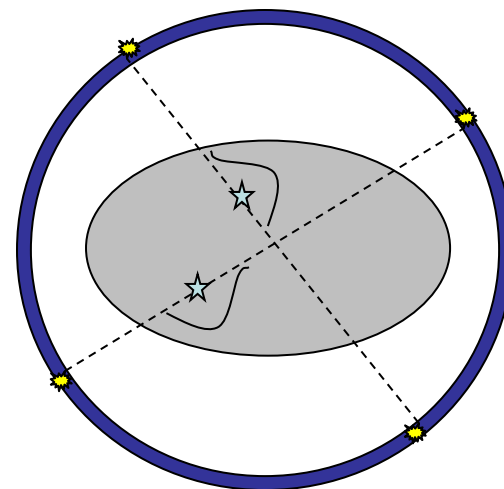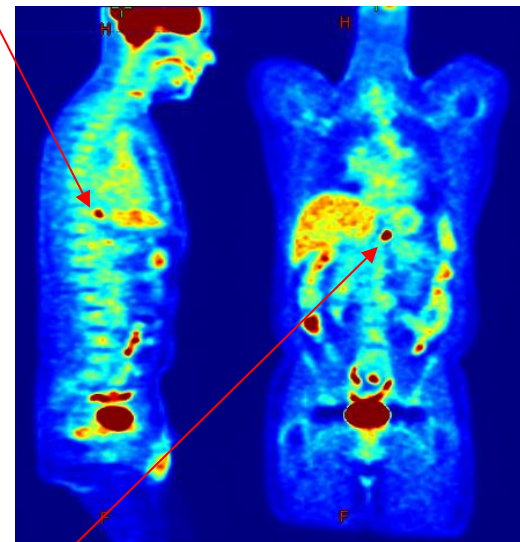
- The most common clinical usage of PET is in Oncology
  - Most used radiotracer is [18F]FDG
    - 18F-Fluor-Deoxy-Glucose
    - Similar structure to sugar
      - High uptake in cells with a high metabolic activity
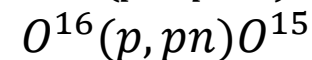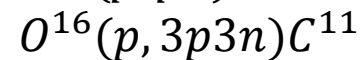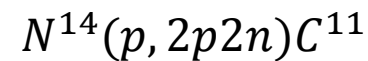   - Typically used for target identification and cancer staging

- [18F]NaF
  - 18F Sodium fluoride is often used to identify sites of metastatic bone disease
    - NaF is preferentially taken into bone depending on the available exposed bone surface
      - More bone surface is exposed for a variety of benign and malignant bone disorders

Far left: 30 mCi 99mTc MDP Bone Scan; Center: 10 mCi F FDG, FDG PET; Far right: 10 mCi 18F NaF,18F NaF PET

https://www.cedars-sinai.org/programs/imaging-center/clinical-trials/nopr-registry/18f-sodium-fluoride-pet-bone-scan.html

- **Proton Dose Deposition Verification**
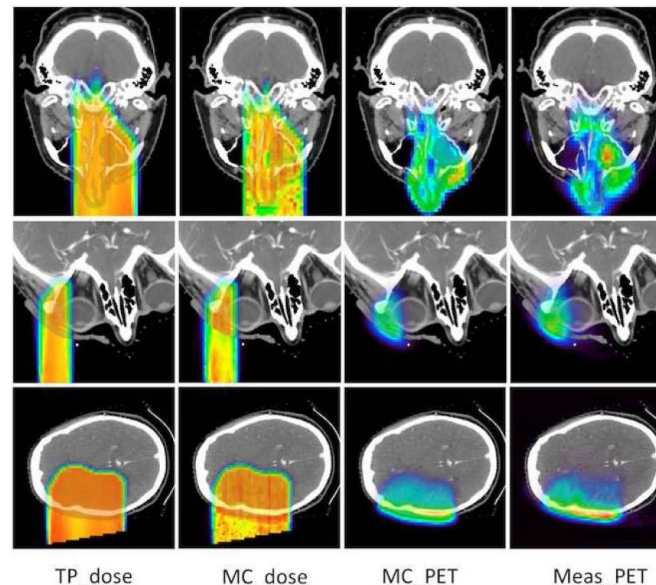 - Proton therapy has gained popularity over the past couple decades
  - Proton interactions with neuclei in tissue have been found to create a number of unstable, β^+ emitting isotopes

$$C^{12}(p, pn)C^{11} \qquad N^{14}(p, 2p2n)C^{11}$$
$$O^{16}(p, 3p3n)C^{11} \qquad O^{16}(p, pn)O^{15}$$
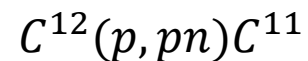
  - Relatively short half-lives of isotopes and logistical difficulties keep this an area of active research

TP_dose   MC_dose   MC_PET   Meas_PET

CH Min, et. al. "Clinical Application of in-room PET for in-vivo Treatment Monitoring in Proton Radiotherapy" Int J Radiat Oncol Biol Phys 2013 May 1; 86(1): 183-189 doi: 10.1016/j.ijrobp.2012.12.010

- Biologically Guided Radiotherapy (BGRT)
  - Utilizes PET signal as an internal marker for radiotherapy delivery
    - Provide internal target motion tracking
      - Lung Stereotactic Body Radiotherapy
  - Provide internal tumor tracking
    - Conventional Radiotherapy gives a uniform dose to the entire tumor
    - PET guidance can reveal different metabolic functions of a tumor allowing for adaptive radiotherapy
      - Necrotic regions
        - Cells have already died and do not need to be targeted
      - Hypoxic regions
        - Cells have a low oxygen saturation and are more radio-resistant
      - Highly metabolic regions
   - Cells are proliferating and are more radio-sensitive

Magnetic Resonance Imaging

- Clinical applications of MRI are largely based on magnetic properties of the hydrogen nucleus
  - Biological tissue is mostly made of water providing a large number of hydrogen nuclei

- Unpaired nucleons in an atomic nucleus will result in a net magnetic moment
  - Protons and Nucleons create "opposite" magnetic fields which, when paired, result in an "essentially' zero magnetic moment
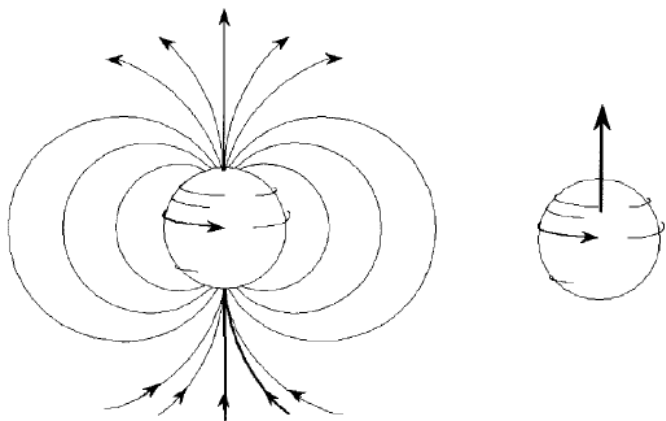
Nucleus	Spin Quantum Number	% Isotopic Abundance	Magnetic Moment	Relative Concentration	Relative Sensitivity
^{1}H	1/2	99.98	2.79	100	1
^{16}O	0	99	0	50	0
^{17}O	5/2	0.04	1.89	50	0.000009
^{19}F	1/2	100	2.63	0.000004	0.00000003
^{23}Na	3/2	100	2.22	0.08	0.0001
^{31}P	1/2	100	1.13	0.075	0.00006

JT Bushberg, JA Anthony, EM Leidholdt, JR., JM Boon. *The Essential Physics of Medical Imaging*. Lipincott Williams & Wilkins, Philadelphia, USA 2002

- In normal circumstances, the magnetic moment from individual nuclei is oriented randomly

    - Results in no net magnetization

- When an external magnetic field is applied, the magnetic dipole will align with the magnetic field lines

    - Two energy states are possible

        - $E_{pot} = -\mu \cdot B = \mp \frac{1}{2} \gamma \hbar B$

    - Ratio of nucleons in spin up vs. spin down states follows the Boltzmann Distribution

        - $\frac{N_\downarrow}{N_\uparrow} = e^{-\Delta E_{pot}/kT} = e^{-\gamma \hbar B/kT}$

- Population difference results in a net magnetization

    - Referred to as M_0 in following slides

E_{pot}

$\frac{1}{2} \gamma \hbar B$

$-\frac{1}{2} \gamma \hbar B$

B_0
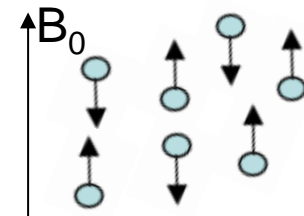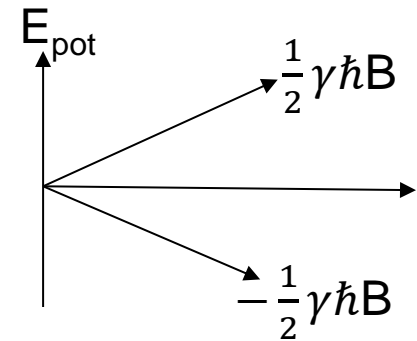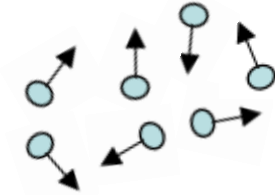
- Additionally, a proton will precess about the axis of the external magnetic field
  - Precession frequency is given by the Larmor frequency derived from the Bloch equations
    - $\omega_L = \gamma B$
  - This gives rise to two useful frames of reference
    - Laboratory Frame
      - Stationary system with the z-axis oriented in the direction of the external magnetic field
    - Rotating Frame
      - Coordinate frame rotates about the z-axis, which is oriented in the direction of the external magnetic field
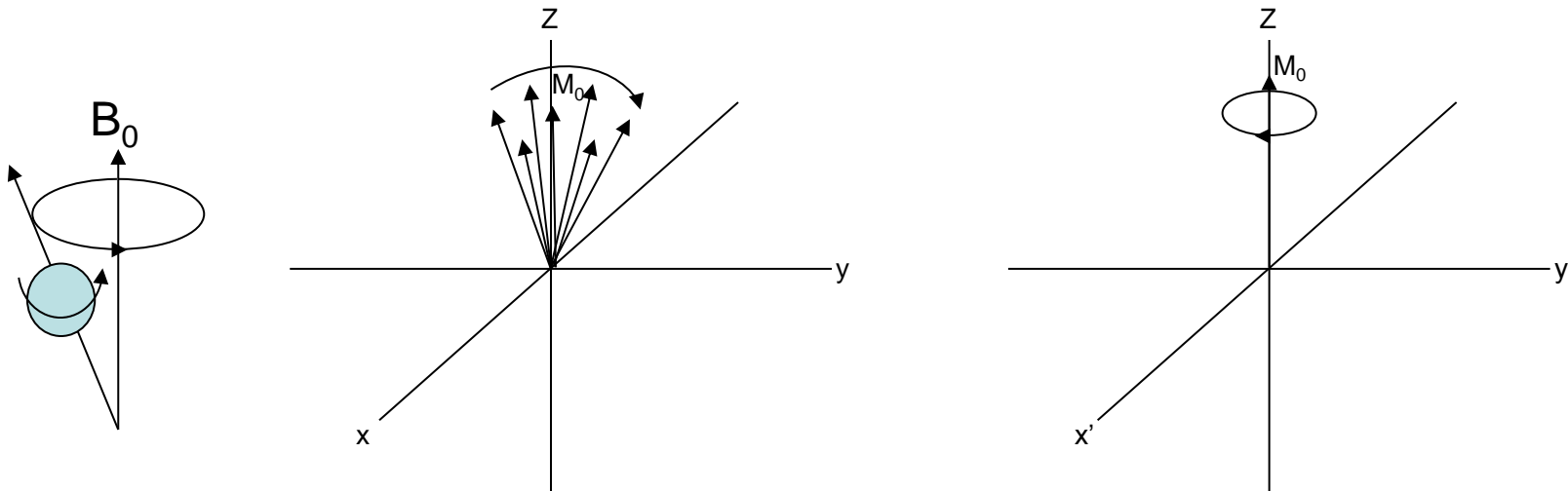
- By introducing a radiofrequency pulse, we can manipulate M_0
  - If the RF pulse is oscillating at the Larmor Frequency, a net tourque is applied to M_0, causing it to "flip"
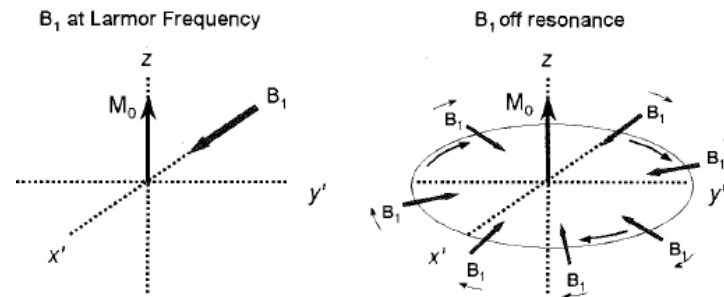

JT Bushberg, JA Anthony, EM Leidholdt, JR., JM Boon. *The Essential Physics of Medical Imaging*. Lipincott Williams & Wilkins, Philadelphia, USA 2002

- The degree at which the magnetization is tipped relative to the external field is derived from Bloch's equations
  - $\theta = 2\pi\gamma\tau B_1$
  - The flip angle is dependent on the power of the RF pulse and its duration
  - 90° and 180° angle are comon
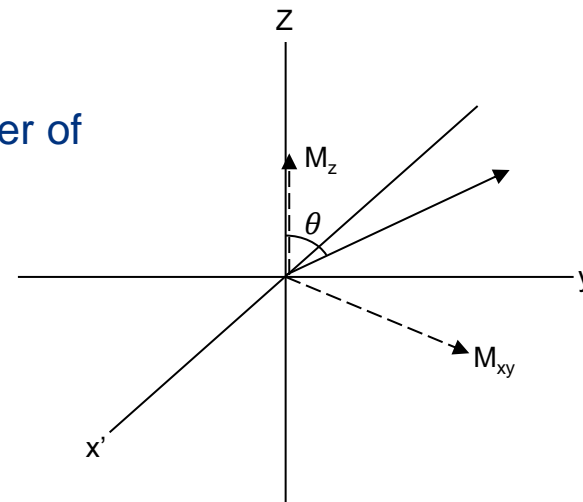
- Decay of M_z is referred to as Longitudinal relaxation, Spin lattice relaxation, or, more commonly, as **T1 relaxation**
  - Describes the re-alignment of the net magnetization with the external magnetic field
  - Different tissues have different rates of relaxation
    - $M_z(t) = M_0\big(1 - e^{-t/T_1}\big)$
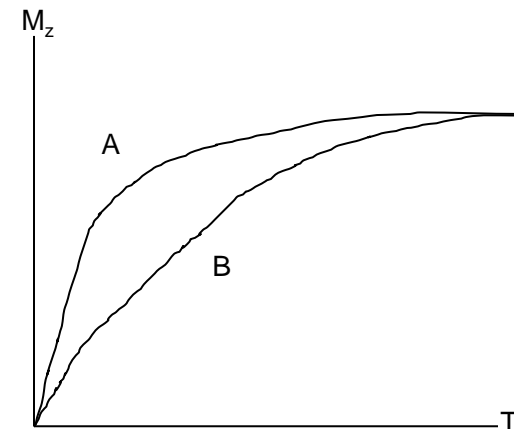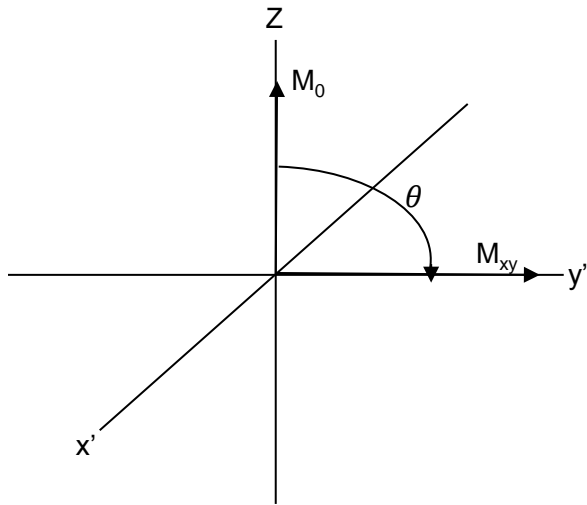
- Decay of M_{xy} is referred to as transverse relaxation, spin-spin relaxation, or T2 relaxations
  - Immediately after the RF pulse all spins are in phase
  - Describes the dephasing between spins
    - Interactions between spins (T_2)
      - Depends on tissue characteristics
    - Interactions with small inhomogeneties in the external magnetic field (T_2*)
      - Depends on tissue characteristics and the external field
    - $M_z(t) = M_0\left(e^{-t/T_2*}\right)$
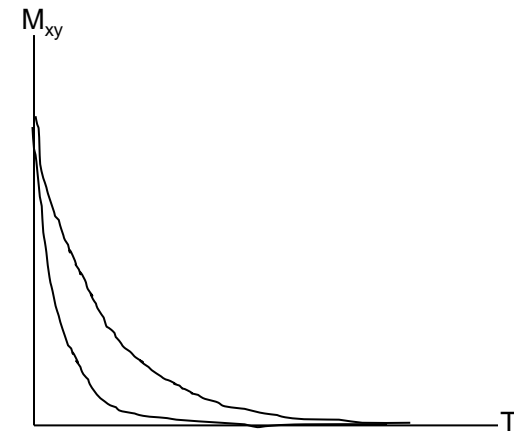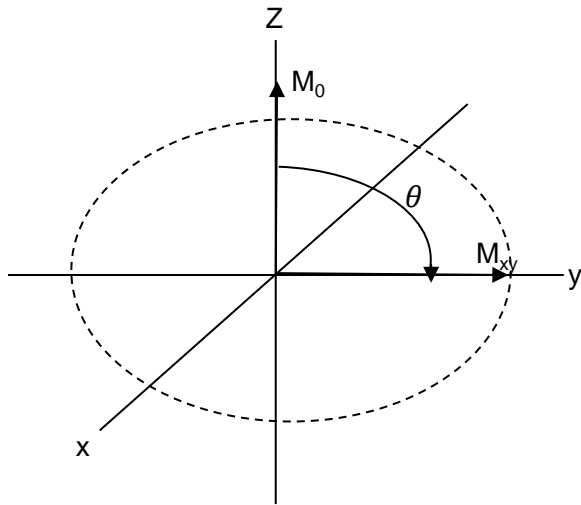
- As the magnetization decays back to equilibrium, that change in magnetization induces a current in a loop of wire
    - Induced signal is known as the Free Induction Decay (FID)
    - Signal strength decays along with the transverse magnetization

- Signal is stored in "k-space"
    - Fourier Transform of k-space results in the MR image
    - Represents the "frequency domain" and a single pixel in k space stores information about every pixel in the image
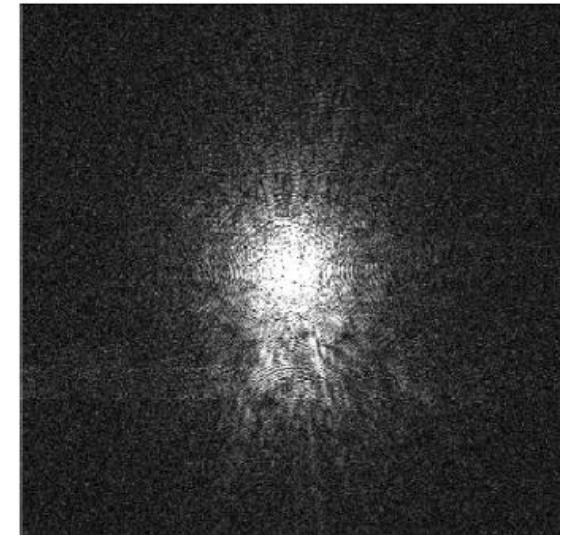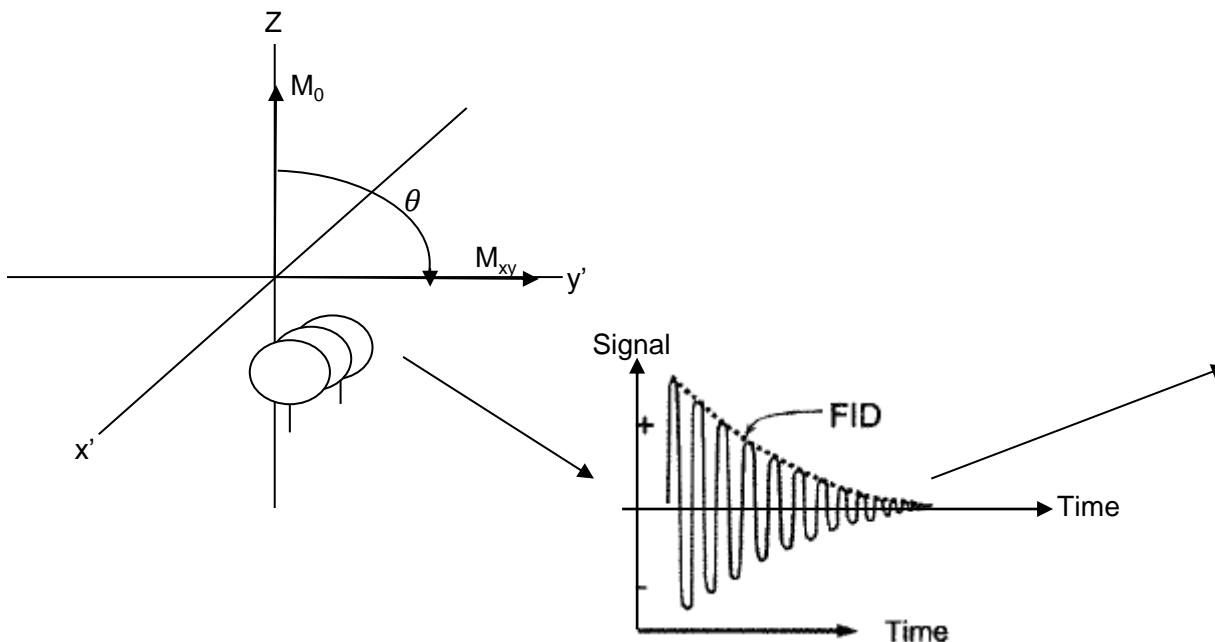

Image from ESTRO 2013 Advanced Imaging for Physicists Lecture Series

- At a constant external field, the received signal would be from the entire volume
  - All protons are precessing at the Larmor Frequency and impacted by the RF signal
  - This provides no spatial information

- In order to obtain spatial information, we need a way to select a set fraction of the volume of interest
  - Apply a gradient to the external field
  - Select bandwidth of the RF pulse

- Slice Selection, G_z
  - A Gradient can be applied in the z-direction which varies the Larmor frequency in the z-direction
    - Steeper gradient results in narrower slice thickness
  - Bandwidth of the RF pulse can be varied to select the slice thickness
    - Narrower bandwidth results in narrower slice thickness
  - Multiple RF pulses are used with varied frequency to select each slice

$$B_0 \pm \Delta B(z)$$

B(z)

$$\omega_0 \pm \Delta\omega$$

Z

	↑	↑
↑	↑	
↑		↑
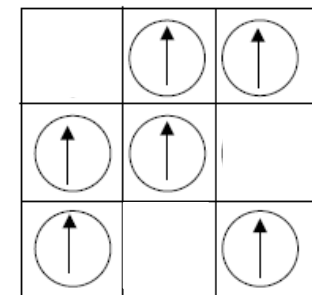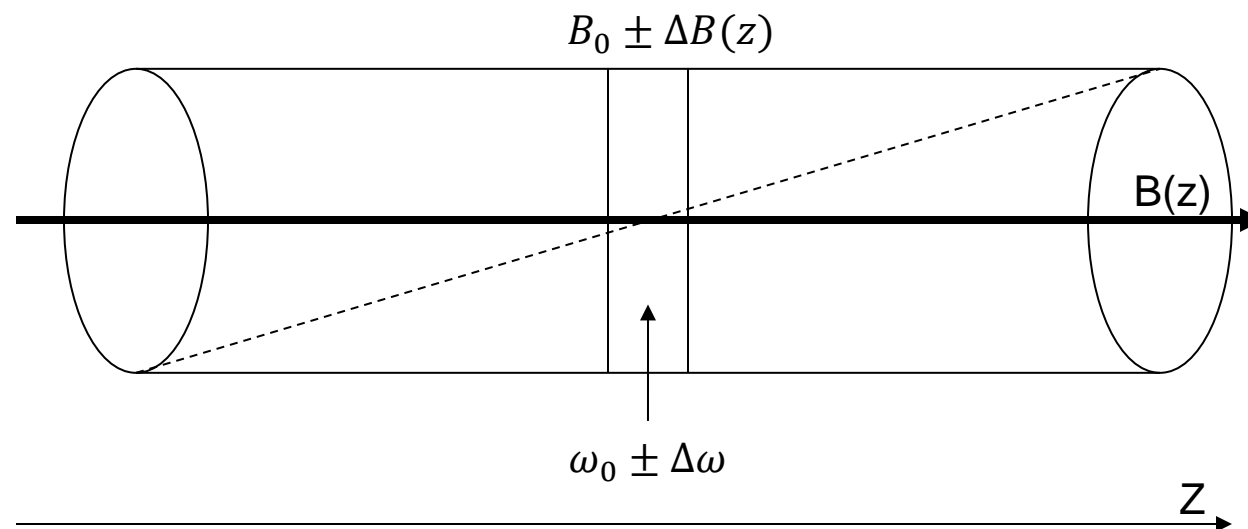
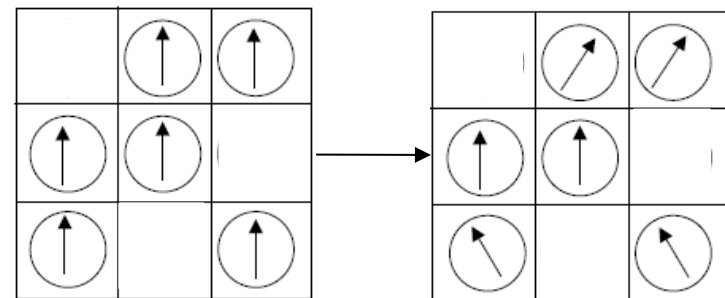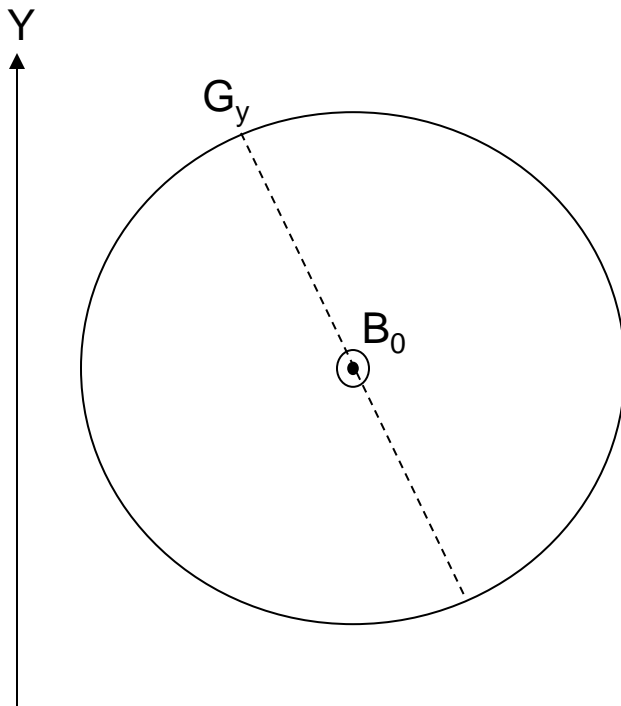| 0	cos (ω₀t)	cos (ω₀t)
cos (ω₀t)	2cos (ω₀t)	0
-2cos (ω₀t)	0	cos (ω₀t)

- Frequency Encoding, G_x
  - Slice gradient narrows the signal to a single plane, but we still need to discriminate the signal in-plane
  - A Gradient can be applied in the x-direction
    - Changes the resonant frequency in the x-direction
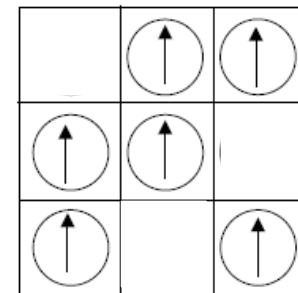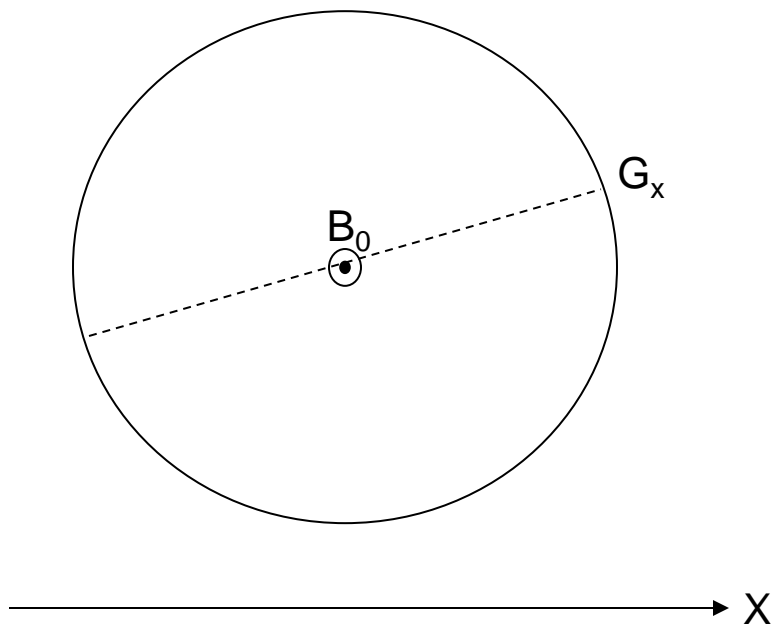
- Phase Encoding, G_y
  - Another gradient is applied in the y direction which changes the phase of each point in the y-direction
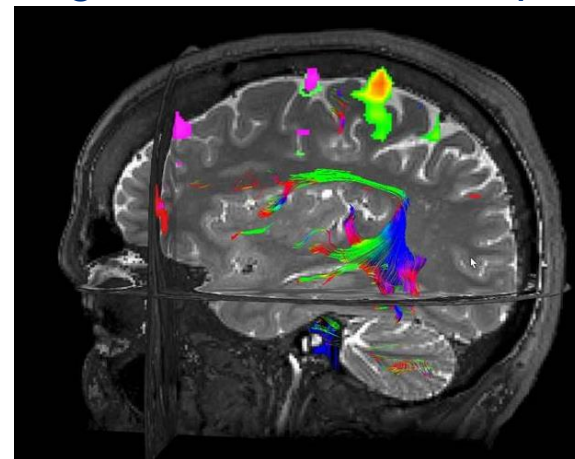
- Functional MRI
  - Common application of MRI in neurological studies
  - Investigates changes in blood flow due to increased neurological activity
    - Listening to music, taping a finger, speaking, etc.
  - Fully oxygenated blood is indistinguishable from surrounding brain tissue, but activation of parts of the brain act to deoxygenate the blood
    - Deoxygenated hemoglobin is highly paramagnetic
  - The deoxygenated blood alters the magnetic field gradients resulting in a difference in T2 and T2* relaxation times
  - Multiple MRI studies are performed during active and inactive periods and activation maps are obtained

Overview of Functional Magnetic Resonance Imaging

Gary H. Glover

https://neurology.ufl.edu/divisions/epilepsy/epilepsy-surgery-program/the-epilepsy-management-conference-emc/functional-magnetic-resonance-imaging-fmri/

- Ultrahigh Magnetic Field Strengths
    - Conventional MRI fields are on the order of 1.5-3 T
    - In recent years, 7 T magnets have become clinically available
    - As of Sept. 2021, the strongest human MRI is 11.7T
    - Signal-to-Noise ratio increases linearly with the external magnetic field strength
        - Allows for more sensitive measurements for more detailed functional imaging
    - Spatial resolution is expected to be <0.3mm at ultrahigh field strengths allowing for better visualization of small structures and their organzation

Toward 20 T magnetic resonance for human brain studies: opportunities for discovery and neuroscience rationale

Thomas F. Budinger,[1] Mark D. Bird,[2] Lucio Frydman,[2,3] Joanna R. Long,[4] Thomas H. Mareci,[4] William D. Rooney,[5] Bruce Rosen,[6] John F. Schenck,[7] Victor D. Schepkin,[2] A. Dean Sherry,[8] Daniel K. Sodickson,[9] Charles S. Springer,[5] Keith R. Thulborn,[11] Kamil Uğurbil,[10] and Lawrence L. Wald[6]

AMERICAN ASSOCIATION of PHYSICISTS IN MEDICINE

THE GLOBAL Research Education And Career coacHing (REACH) is a 10-week virtual undergraduate fellowship designed to provide promising students exposure to the profession of medical physics in Low-to-Middle-Income Countries (LMICs) across the African continent. This fellowship has partnered with the African School of Physics (ASP) to offer research opportunities, outreach, and strategic mentorship geared towards recruiting a robust and diverse group of skilled undergraduate students. Global REACH students will be paired with an AAPM mentor and project that is consistent with their research and career interests. **Two** Global REACH fellows will be selected on a competitive basis and will match with an AAPM mentor. Funding up to $4,300 will be awarded to selected fellows which includes a $1500 fellowship award and travel bursary.

Additionally, we will invite the fellows to attend the 2023 American Association of Physicists in Medicine (AAPM) annual meeting to interact with the mentor and other AAPM members in July 23 -27, 2023 (Houston, Texas)

ELIGIBILITY

- Undergraduate juniors and seniors majoring in physics, engineering, or other science
- Able to have access to reliable internet connections and to perform research under the guidance of a mentor in the USA
- Country of residence is a LMIC as defined by the ASP
- Sufficient ability to communicate in the English language

HOW TO APPLY

- Send an email to 2022.GSPSC@aapm.org to express interest in the program
- The selection committee will respond with the application information
- Return the completed application and all application materials
    - PDF Application, Current Transcripts, One Page Statement of Interest, 1-2 Letters of recommendation, Resume or Curriculum Vitae

APPLICATION DEADLINE:

February 2, 2023

PROGRAM CONTACT: AAPM, 2022.GSPSC@aapm.org . Sponsored by the AAPM International Council through the AAPM Education and Research Fund.